The Abdus Salam
International Centre for Theoretical Physics

United Nations
Educational, Scientific and
Cultural Organization

IAEA
International Atomic Energy Agency

2332-28

School on Synchrotron and FEL Based Methods and their Multi-Disciplinary Applications

19 - 30 March 2012

Exotic states of matter explored with short-wavelength free-electron lasers

Libor Juha
Academy of Sciences of the Czech Republic Prague
Czech Republic

Exotic states of matter explored with short-wavelength free-electron lasers

Libor Juha

Department of Radiation and Chemical Physics
Institute of Physics
Academy of Sciences of the Czech Republic
Prague, Czech Republic

E-mail: juha@fzu.cz

Outline

NANOSCOPY LAB
IP-ASCR-Prague

(a) interaction of intense short-wavelength radiation with matter: sources of motivation; volumetric heating
(b) short-wavelength lasers used for these studies
    (i) plasma-based lasers
    (ii) free-electron lasers
(c) short-wavelength laser ablation and desorption
(d) characterizing the focused beam from its imprints
(e) behaviour of matter in short-wavelength laser microfocus
    (i) soft X-rays (92 eV): FLASH + probing plasma
    (ii) x-rays (1.56-1.83 keV): LCLS
(f) summary

NANOSCOPY LAB
IP-ASCR-Prague

Why interaction of short-wavelength laser radiation with solids should be investigated?

(1) Estimating and minimizing damages to surfaces of high-flux irradiated XUV/X-ray optical elements developed and used for the guiding and focusing of short-wavelength laser beams as well as those used for long-term irradiation with high repetition rate sources,
(2) durability assessments of materials suggested for the first walls of ICF reactors and optical elements exposed to intense X-ray radiation in a laser-plasma interaction chamber,
(3) diffraction-limited ultrastructuring and patterning of solid surfaces for fabrication of microelectronic and micromechanical elements and devices,
(4) determination of radiation field characteristics: imaging of spatial energy distribution in a focused beam ablatively imprinted on the irradiated material and determination of pulse energy content, and
(5) production of very dense plasmas with T_e ~ 10 eV (WDM - warm dense matter) and T_e ~ 100 eV (HDM - hot dense matter).

Warm Dense Matter - WDM

Nonideal character of plasma is usually characterized by the coupling parameter mentioned by S. Pascarelli last Thursday.

$$\Gamma = \frac{U}{E_k} \simeq 1$$

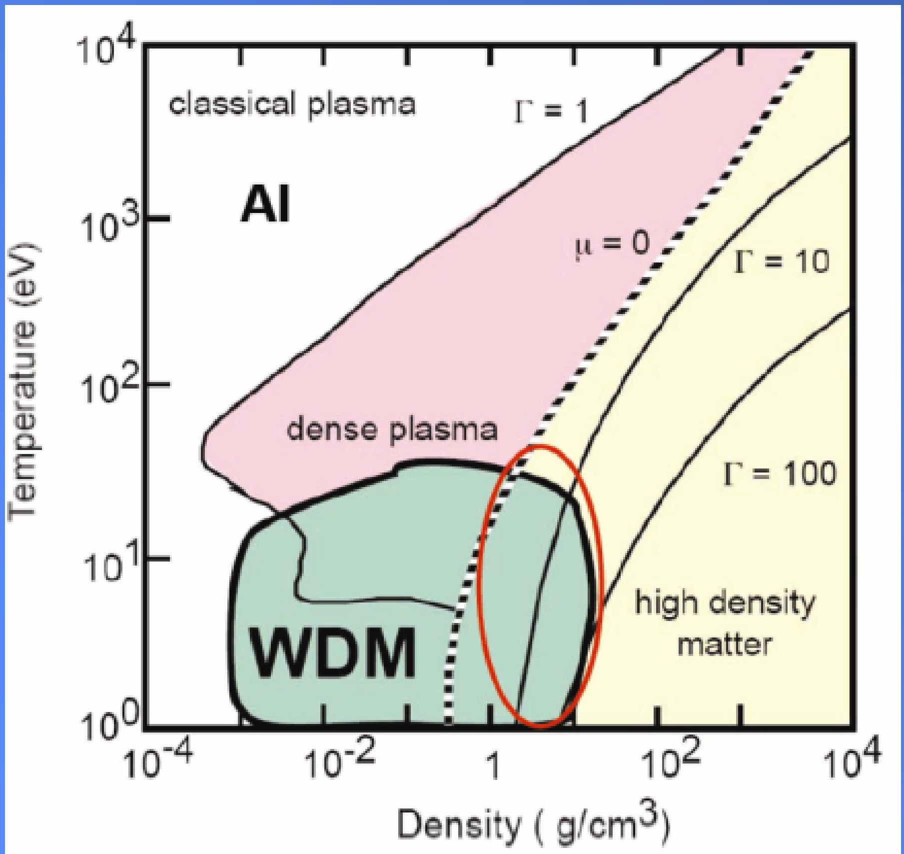

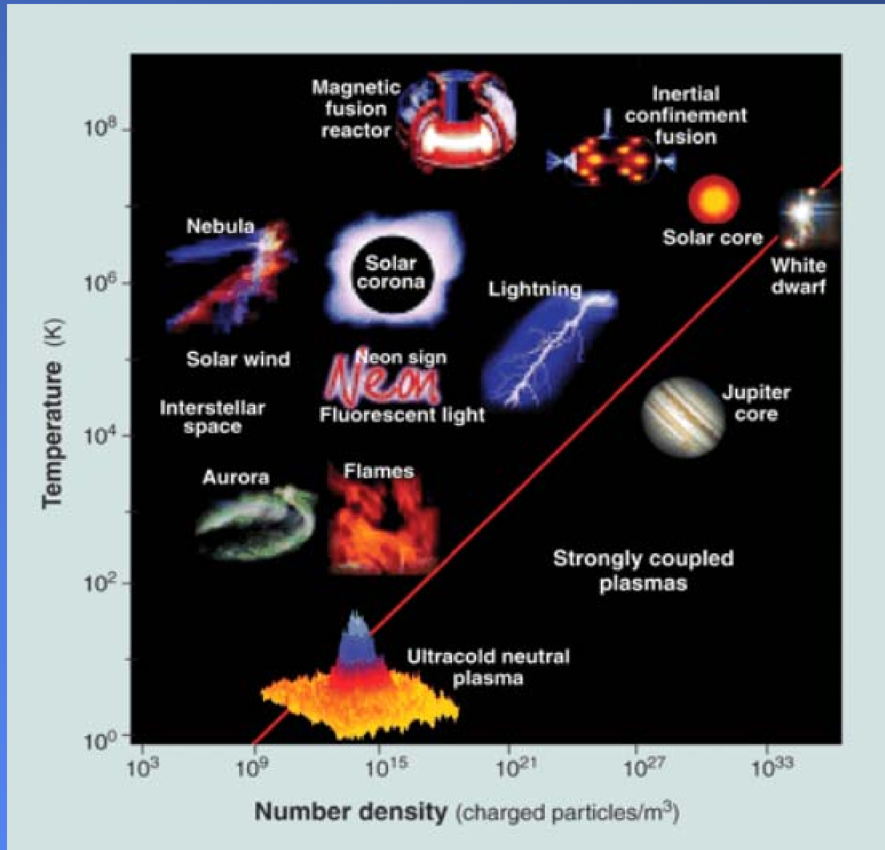

volumetric heating

In certain position, where the frequency of electrons oscillating in plasma (plasma frequency; Langmuir frequency) is equal to the frequency of the laser EM field, the index of refraction of the plasma becomes zero. Thus the EM wave cannot penetrate into the plasma, being reflected. This is called plasma mirror effect.

The plasma frequency is a function of the plasma electron density

$$\omega_e{}^2 = n_e\, e^2 / \varepsilon_0\, m_e$$

and the laser frequency is equal to the plasma frequency exactly at the critical electron density

$$n_c\ [\text{electrons/cm}^3] = 10^{21} \times \lambda^{-2}\ [\mu\text{m}]$$

for λ < 10 nm is $n_c > 10^{25}$ cm^{-3}

$\Rightarrow$ X-rays do not create a critically dense plasma so that their energy is deposited in a volume below the irradiated solid surface

(Dessin de Fernando Cunha)

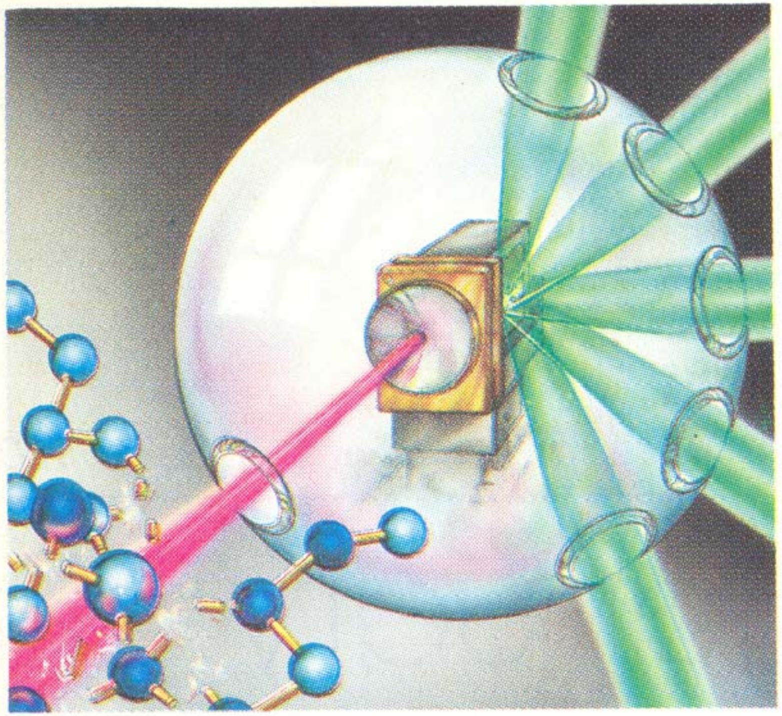

Casser des molécules, une des éventuelles applications du laser X. (p. 16)

P. Jaeglé: Le laser à rayons X, *La Recherche* (184), 16-25 (Jan. 1987).

…decomposition of molecules, one of possible applications of X-ray lasers

Neon-like zinc XRL driven by multi-100-ps IR laser pulses

NANOSCOPY LAB
IP-ASCR-Prague

Simplified level scheme of neon-like zinc

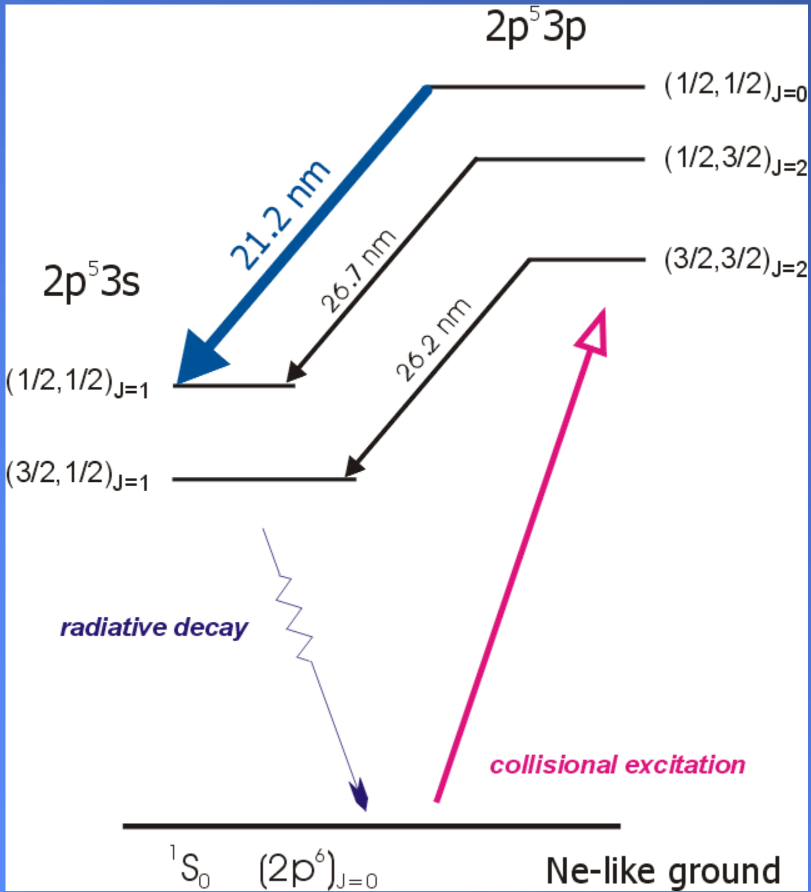

Generic experimental scheme

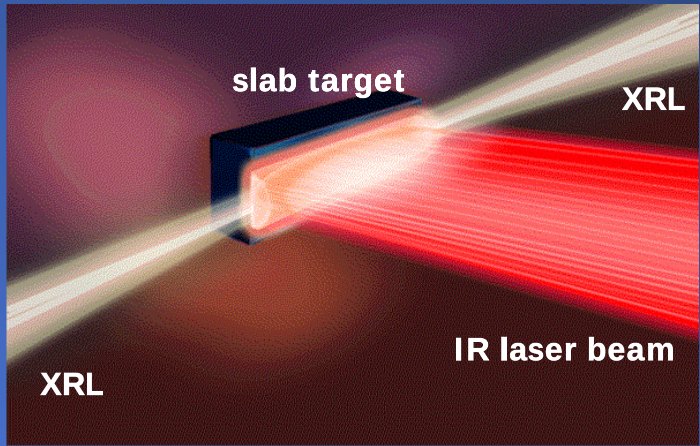

Active medium: a plasma column created from slab target by linearly focused IR laser beam

PALS (Prague Asterix Laser System)

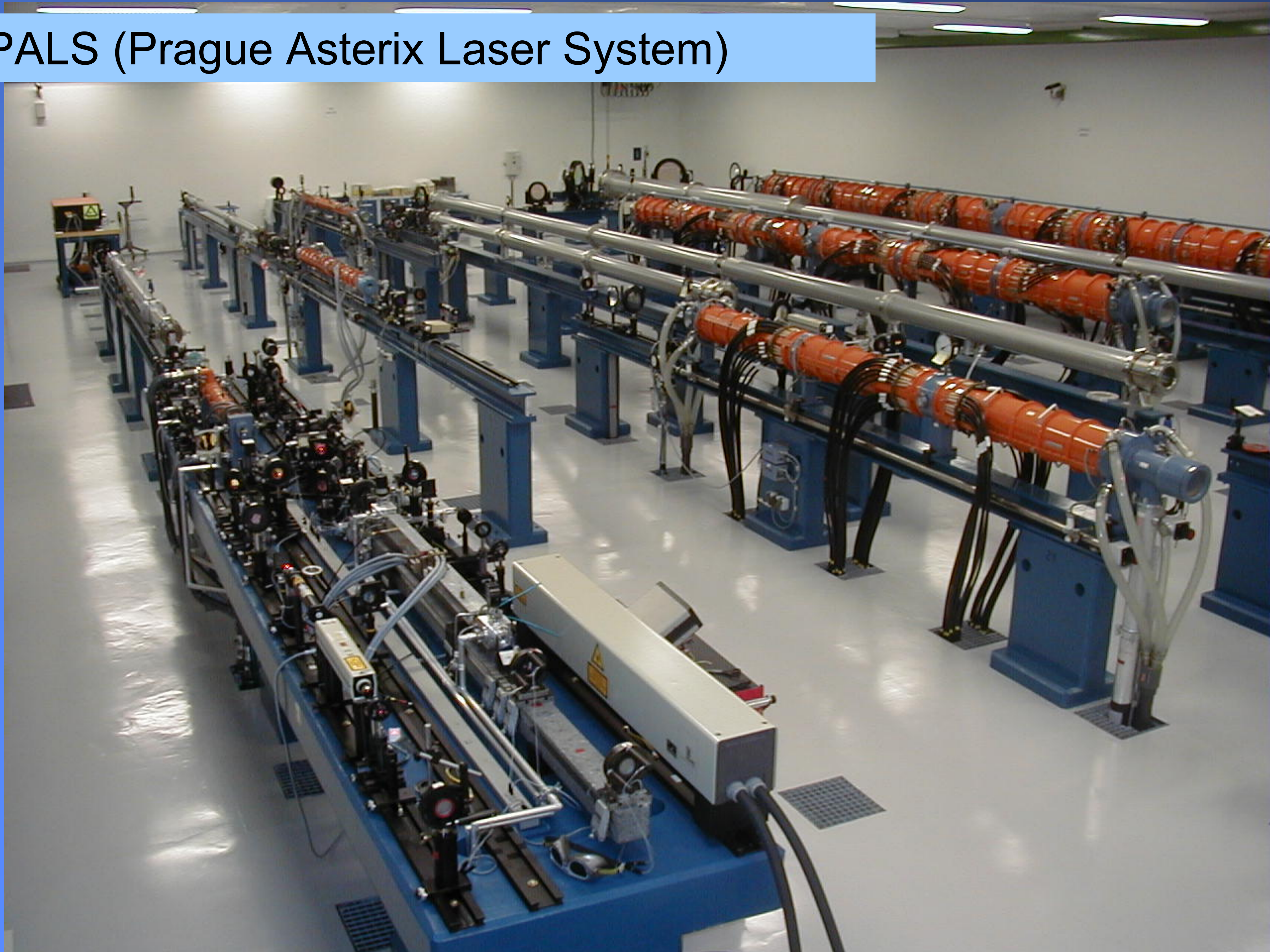

PALS (Prague Asterix Laser System)

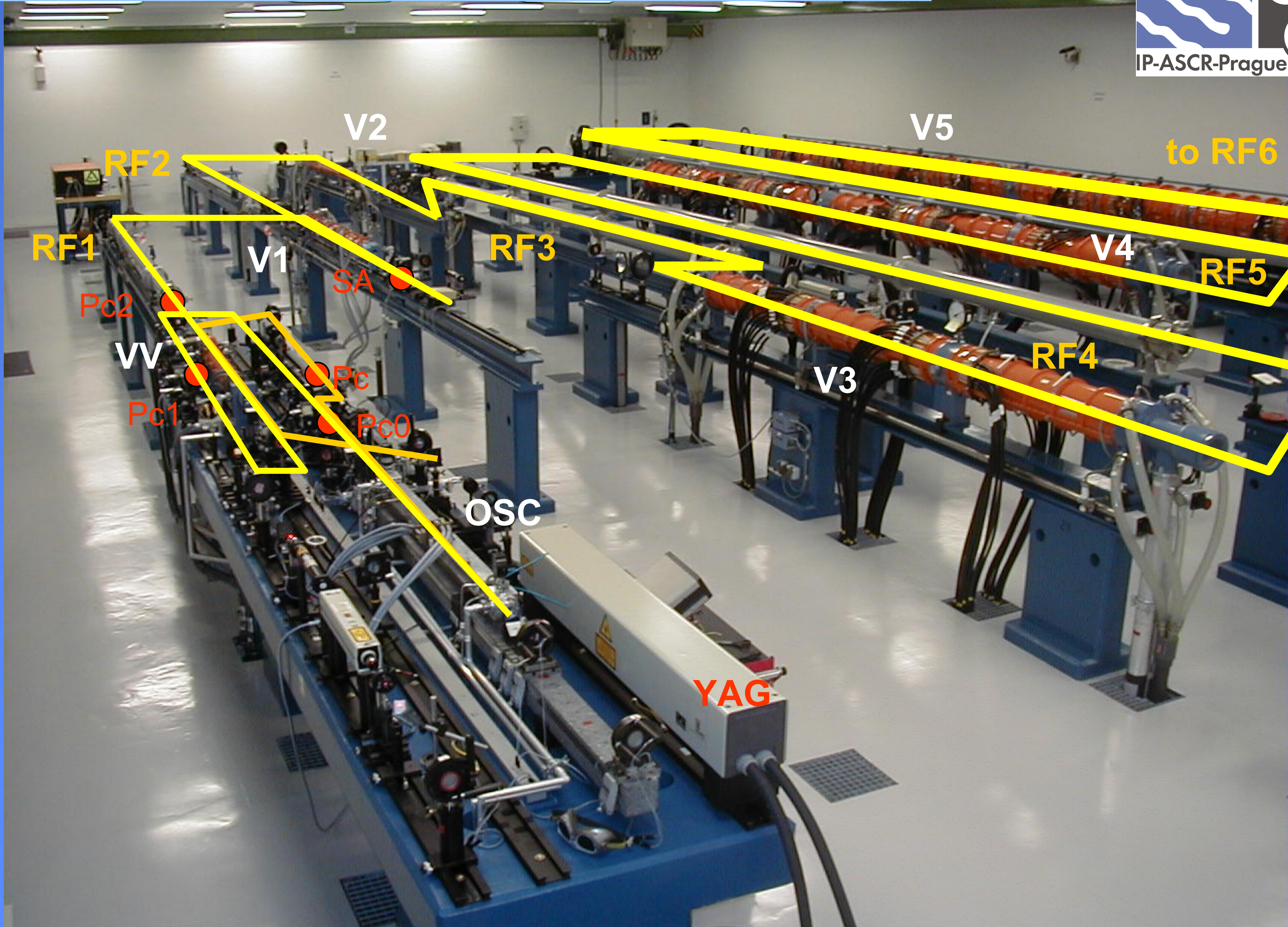

PALS target chambers from the front

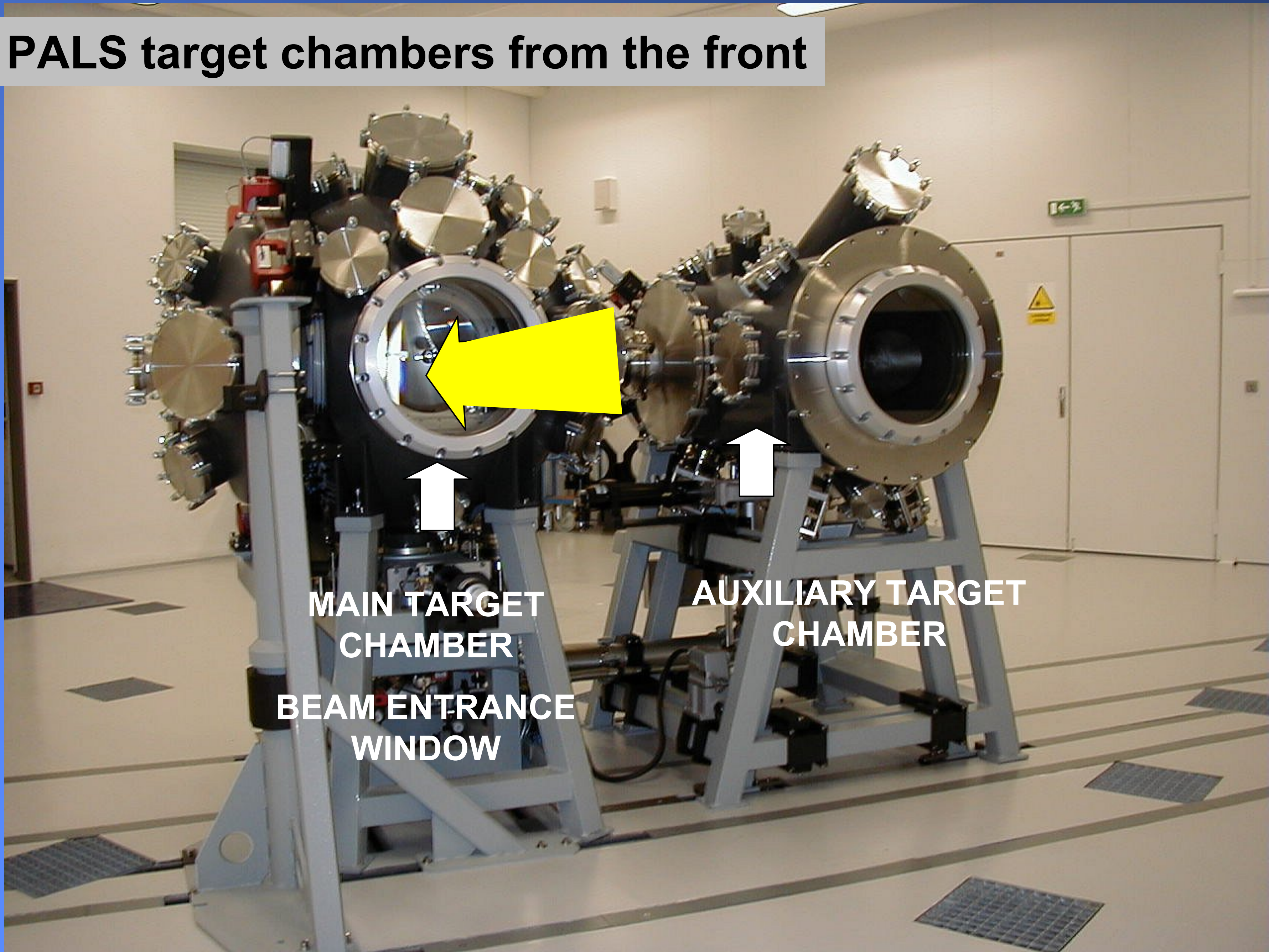

Composite linear focusing optics with 30-mm clear aperture

NANOSCOPY LAB
IP-ASCR-Prague

A novel arrangement: matrix of 10 cylindrical lenses 150x60 mm + single f#3 aspherical lens

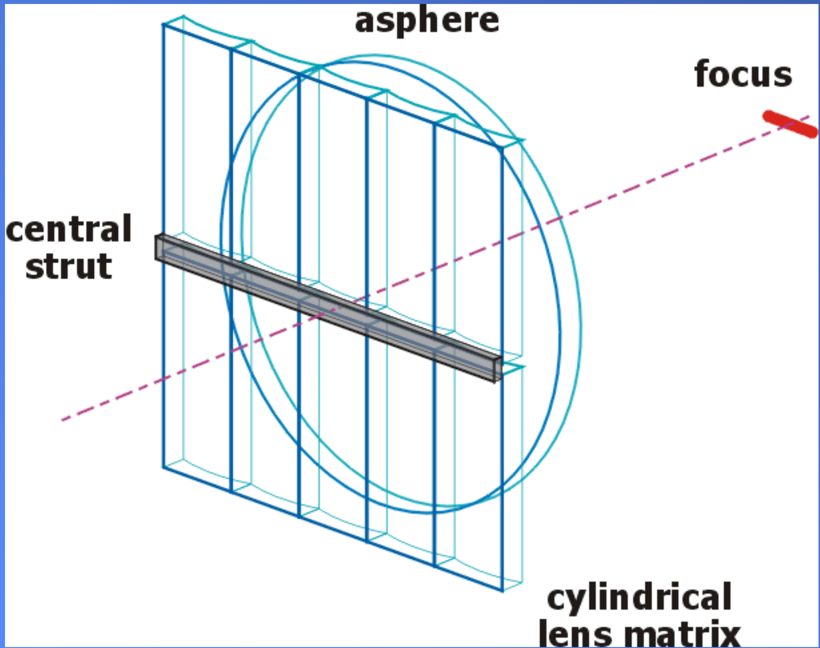

Smaller cylindrical segments may be fabricated <u>very precisely</u> for a <u>moderate cost</u> !

highly uniform & laterally tight linear focus

XRL driving conditions: plasma keV self-emission

Prepulse

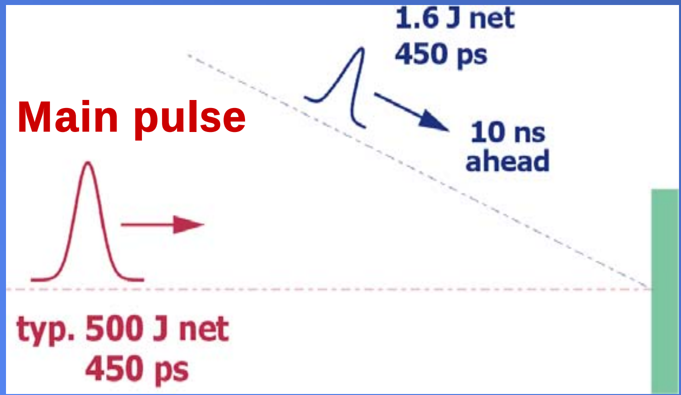

Prepulse: ~1.6×10^{10} Wcm^{-2}

single cylindrical + spherical lens
deliberately de-focused

Main pulse: ~2.8×10^{13} Wcm^{-2}

composite optics: high-quality line focus

Cross-slit X-ray camera data

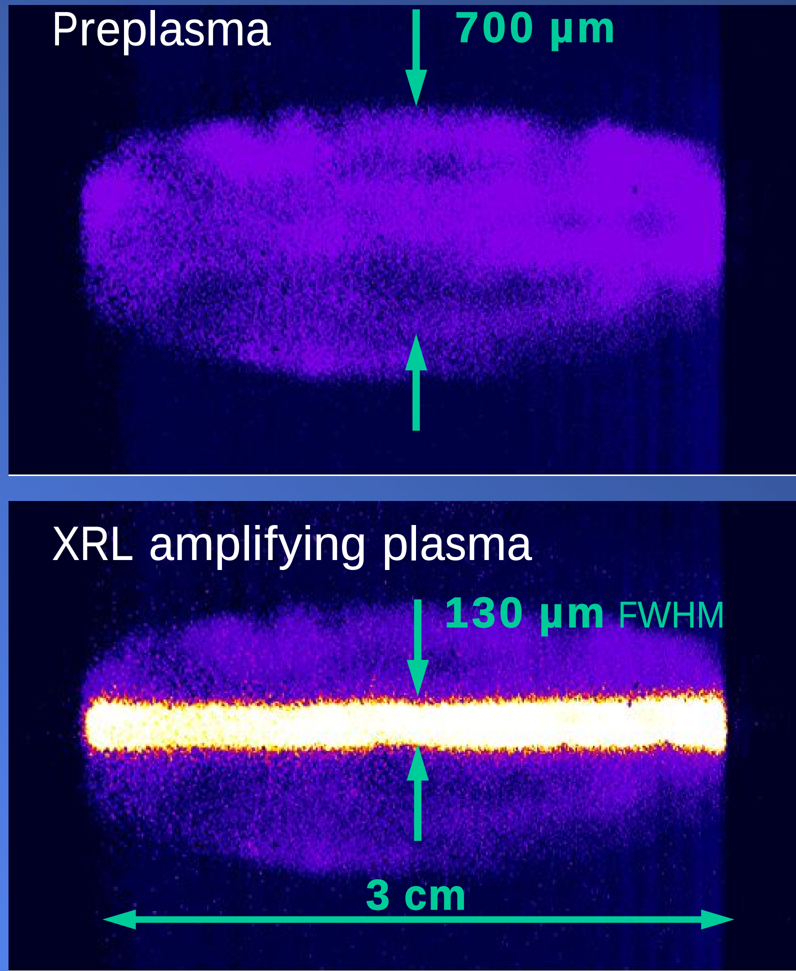

NANOSCOPY LAB
IP-ASCR-Prague

Summary of parameters of the Ne-like Zn laser

Wavelength ⇔ $h\nu$	21.22 nm ⇔ 58.53 eV
XRL pulse energy	**4 mJ**
XRL pulse length	**80-100 ps**
Peak power	**40 MW**
Photons per pulse	$\mathbf{3\times10^{14}}$
Brightness* ($\Delta\lambda/\lambda$=0.001)	10^{27} phot s^{-1} mm^{-2} $mrad^{-2}$
No. of shots with one "batch"	~**100**

$$\text{* Brightness (brilliance)} = \frac{\text{No. of “monochromatic” photons } (\Delta\lambda/\lambda=10^{-3})}{\text{sec} \times \text{surface unit} \times \text{solid angle unit}}$$

focusing scheme of Ne-like Zn soft x-ray laser

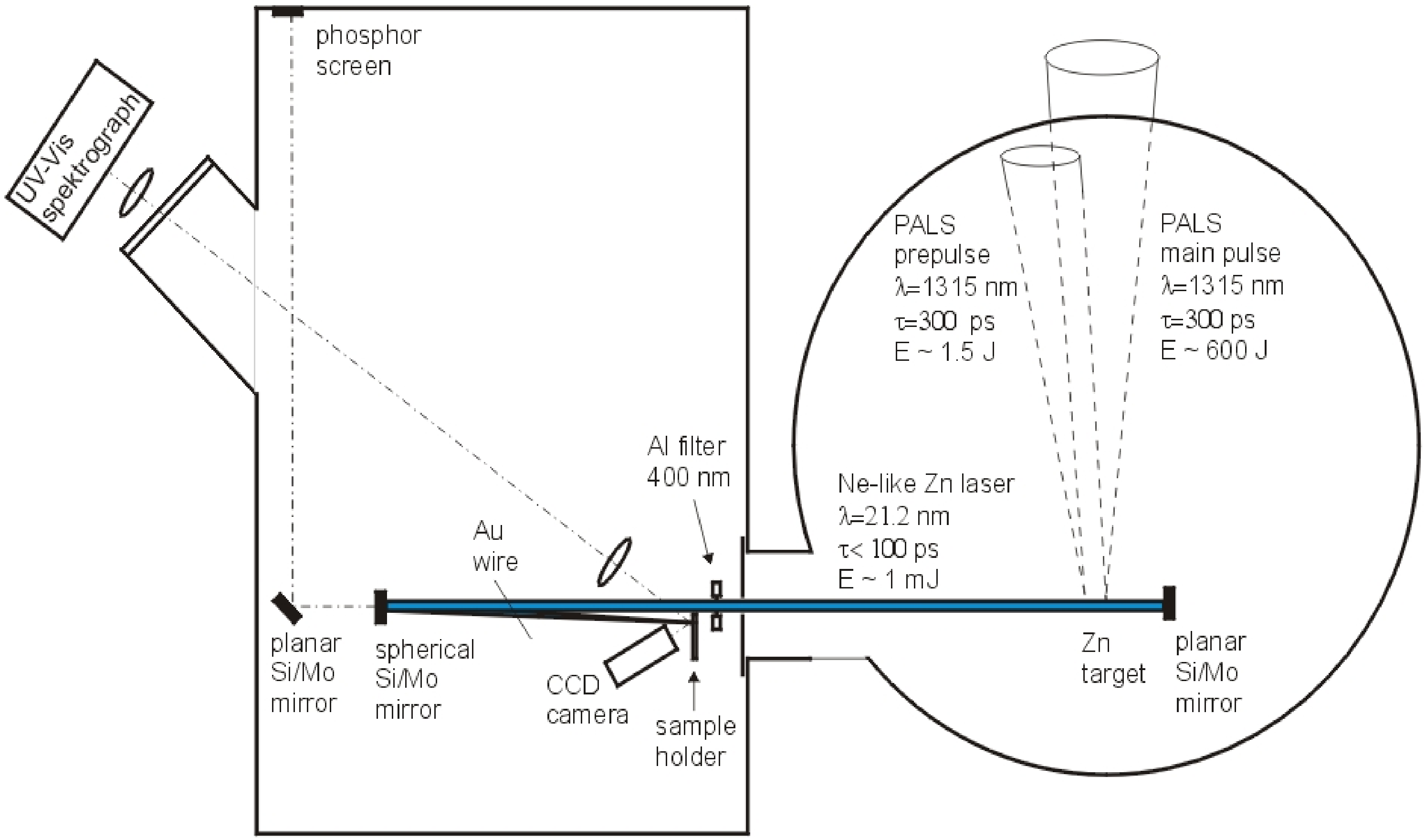

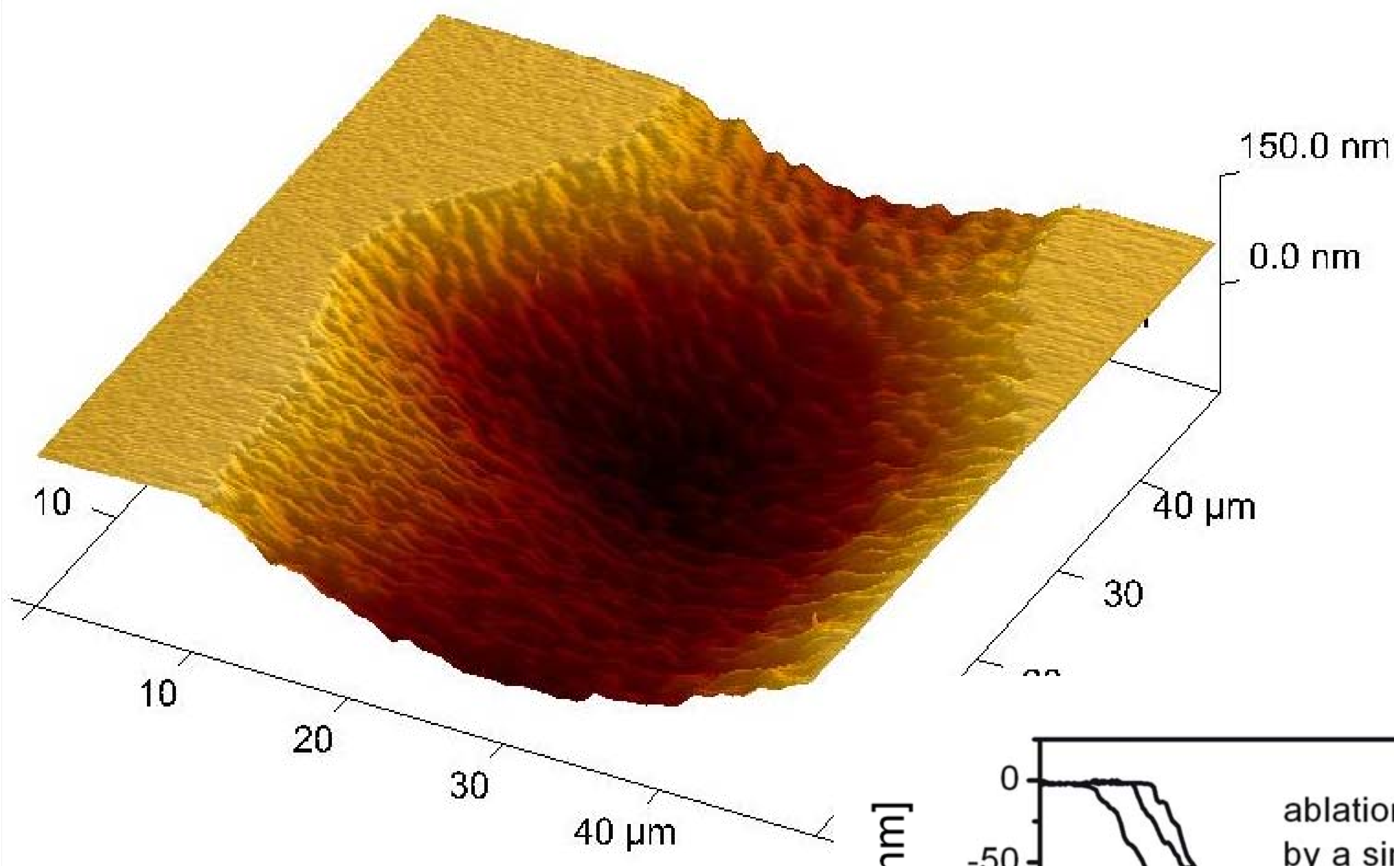

AFM image of crater ablated in PMMA by a focused beam of 21.2-nm laser radiation.

J. Microlith. Microfab. Microsyst. **4**, 033007 (2005)

Appl. Phys. Lett. **89**, 051501 (2006)

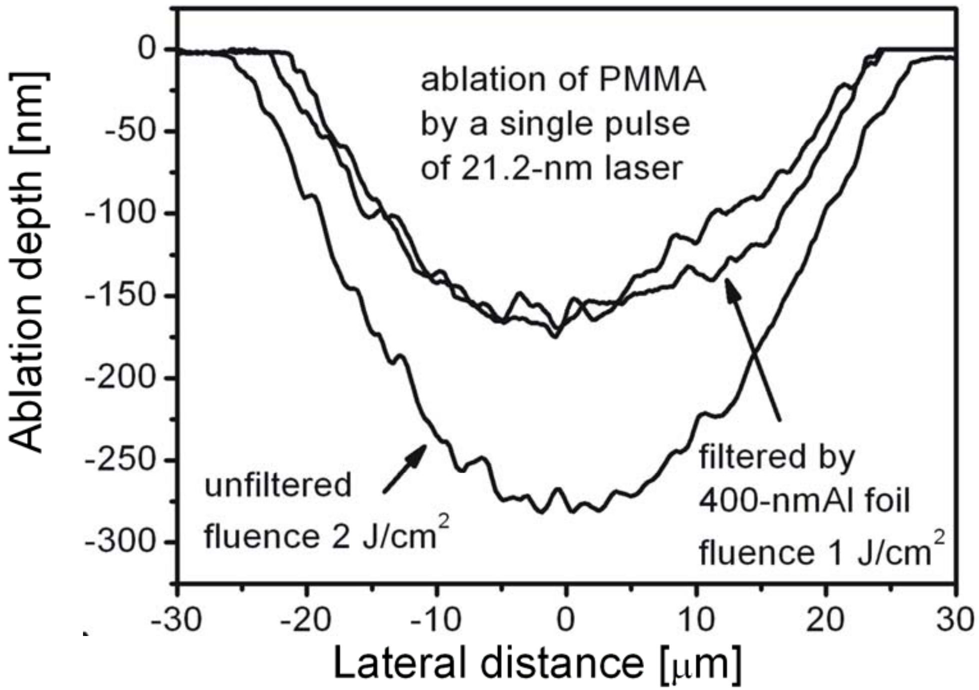

table-top capillary-discharge XUV laser

[made in Fort Collins, Colorado State University –
S. Heinbuch et al.: *Opt. Express* **13**, 4050 (2006)]

NANOSCOPY LAB
IP-ASCR-Prague

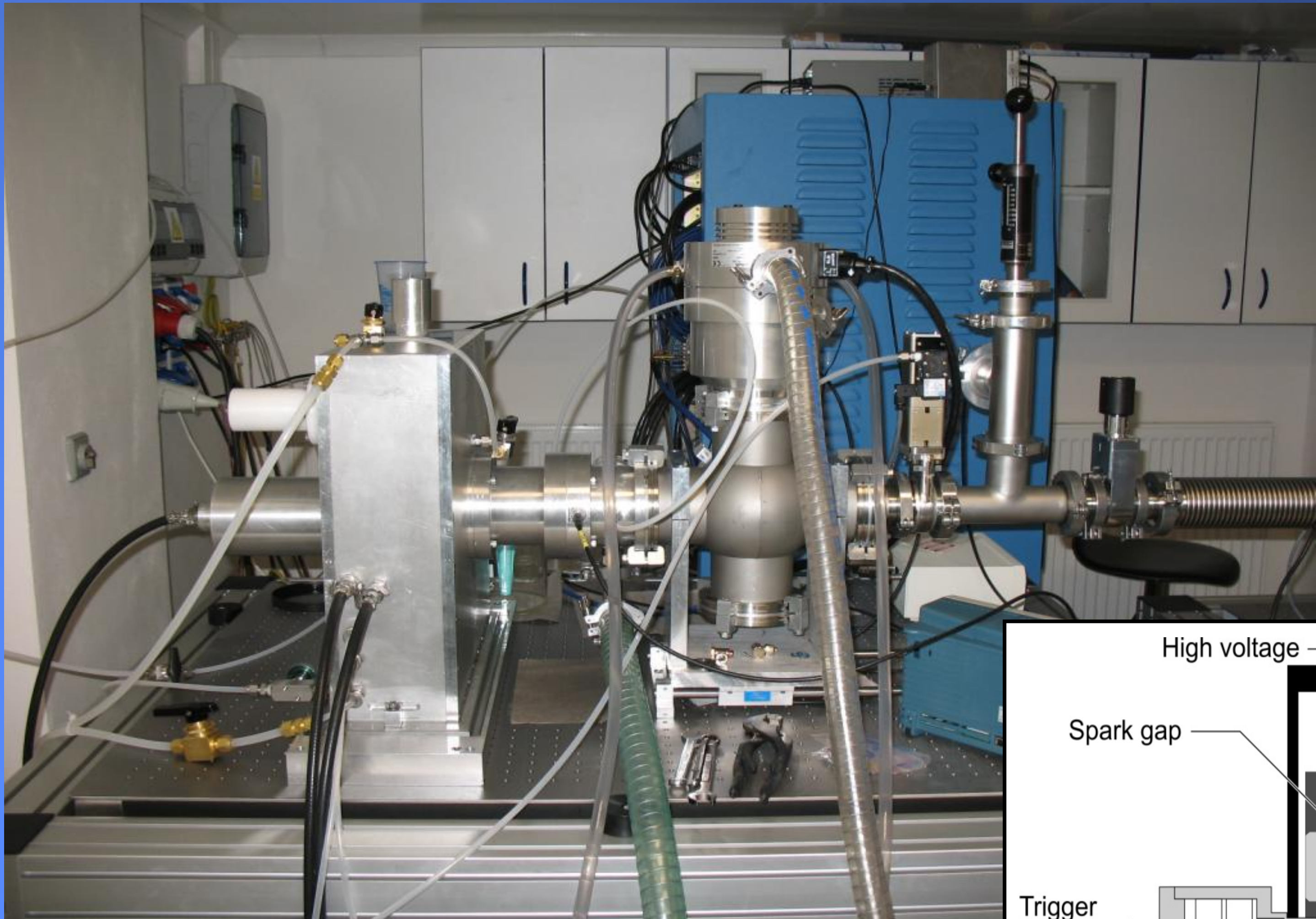

46.9 nm
0.01 mJ
1-2 ns
10 Hz

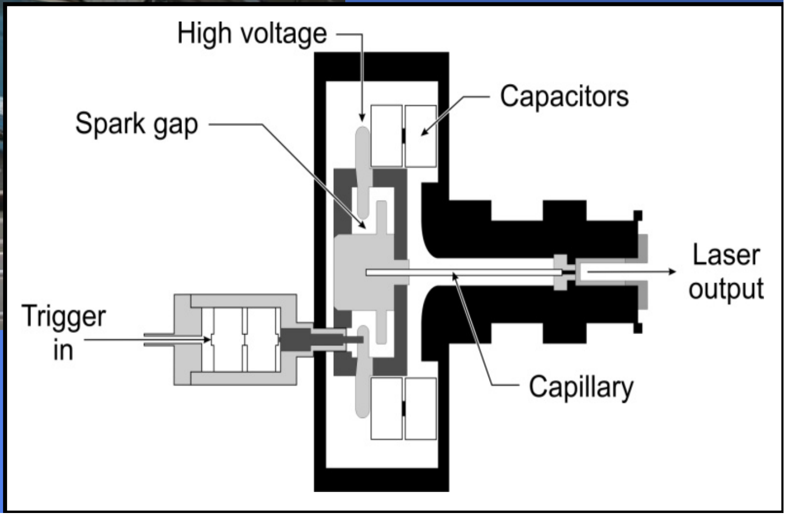

installed in Prague

Focusing the CDL beam

- spherical Sc/Si multilayer mirror (f = 0.25 m) with maximum reflectivity at 46.9 nm
- angle between the incident and reflected beams was about 6°
- sample holder with the target was placed in 3D positioning stage
- irradiated samples of PMMA poly(methyl methacrylate) were illuminated and observed with CCD camera equipped with a magnifying objective

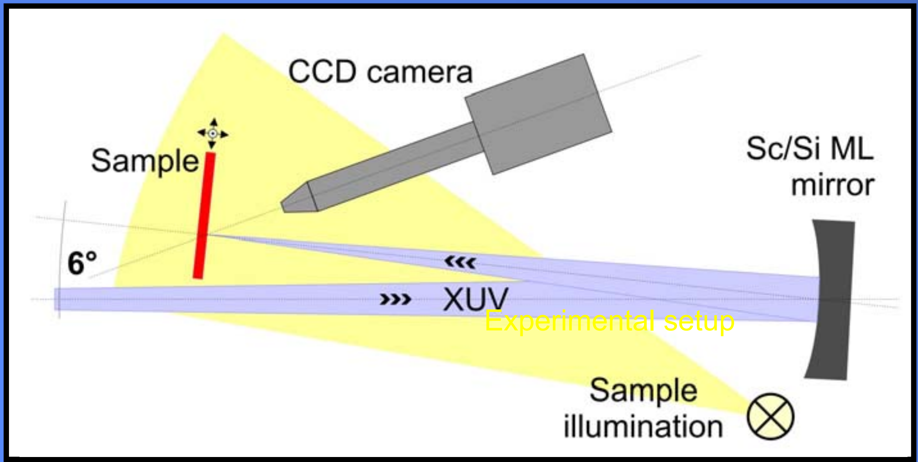

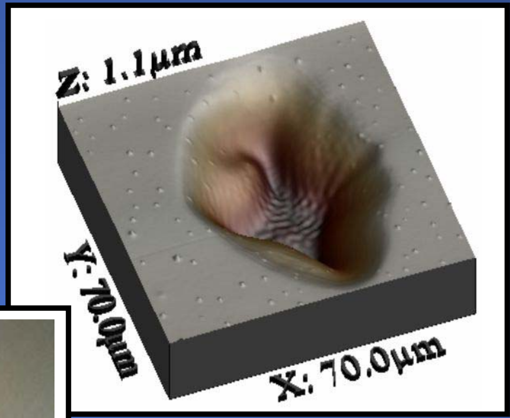

AFM image

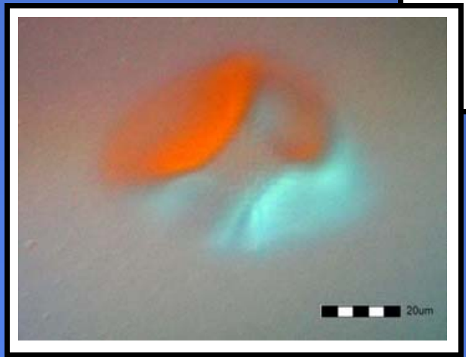

DIC image

- 15 shots for were accumulated

FLASH - Free-electron LASer in Hamburg

TESLA Test Facility
(TTF 1 FEL, 1995-2002)

FLASH, 2005

experimental hall

Photon energy	~30-300 eV
Bandwidth $\Delta\lambda/\lambda$	~0.5 %
Peak power	>1 GW
Pulse duration	~10-100 fs

The European X-Ray Free-Electron Laser

Technical design report

XFEL

X-Ray Free-Electron Laser

1 Introduction

This Technical Design Report of the European X-Ray Free-Electron Laser (XFEL) Facility has been prepared by a large community of scientists and engineers and was edited at Deutsches Elektronen-Synchrotron (DESY) laboratory under the supervision of the European XFEL Project Team.

J. Krzywinski a kol.:

Conductors, semiconductors and insulators irradiated with short-wavelength free-electron laser,

J. Appl. Phys. 101, 043107 (2007)

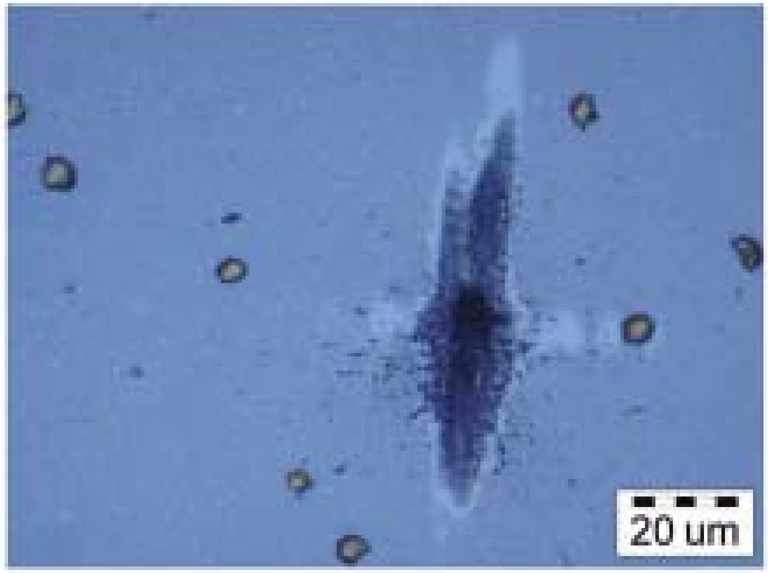

Figure 1.2.1 *Interaction of powerful Vacuum Ultraviolet (VUV) radiation with solids [1-1]. Ablation of Gold target after one pulse of the VUV Self-Amplified Spontaneous Emission (SASE) FEL at the TESLA Test Facility (TTF) at DESY. Radiation wavelength is 98 nm, pulse duration is 40 fs, peak power density is about 100 TW/cm².*

References

[1-1] L. Juha et al., *Ablation of various materials with intense XUV radiation*, Nucl. Instrum. and Methods A 507 (2003) 577.

FLASH experimental hall

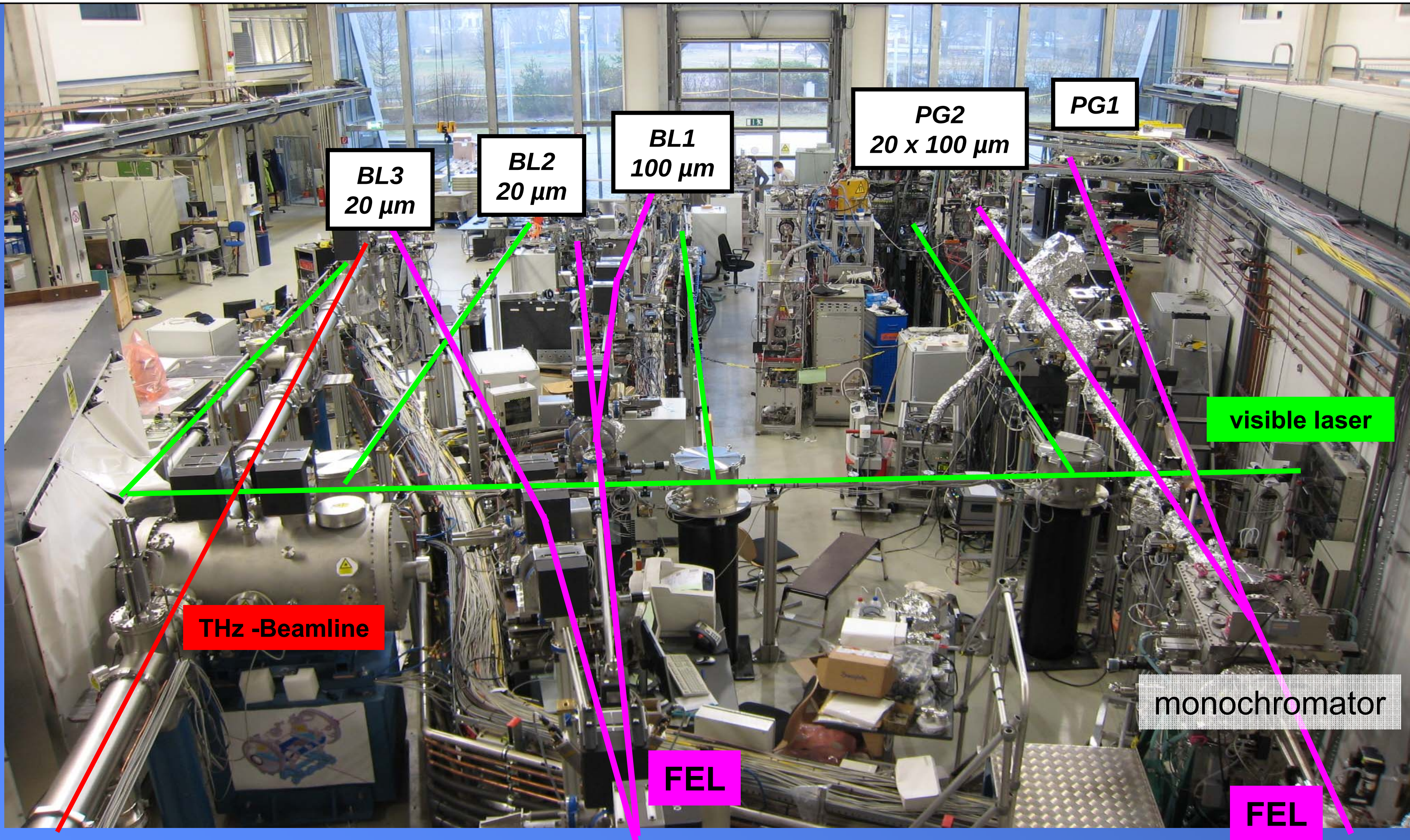

K. Tiedtke et al.: New J. Phys. 11, 023029 (2009)

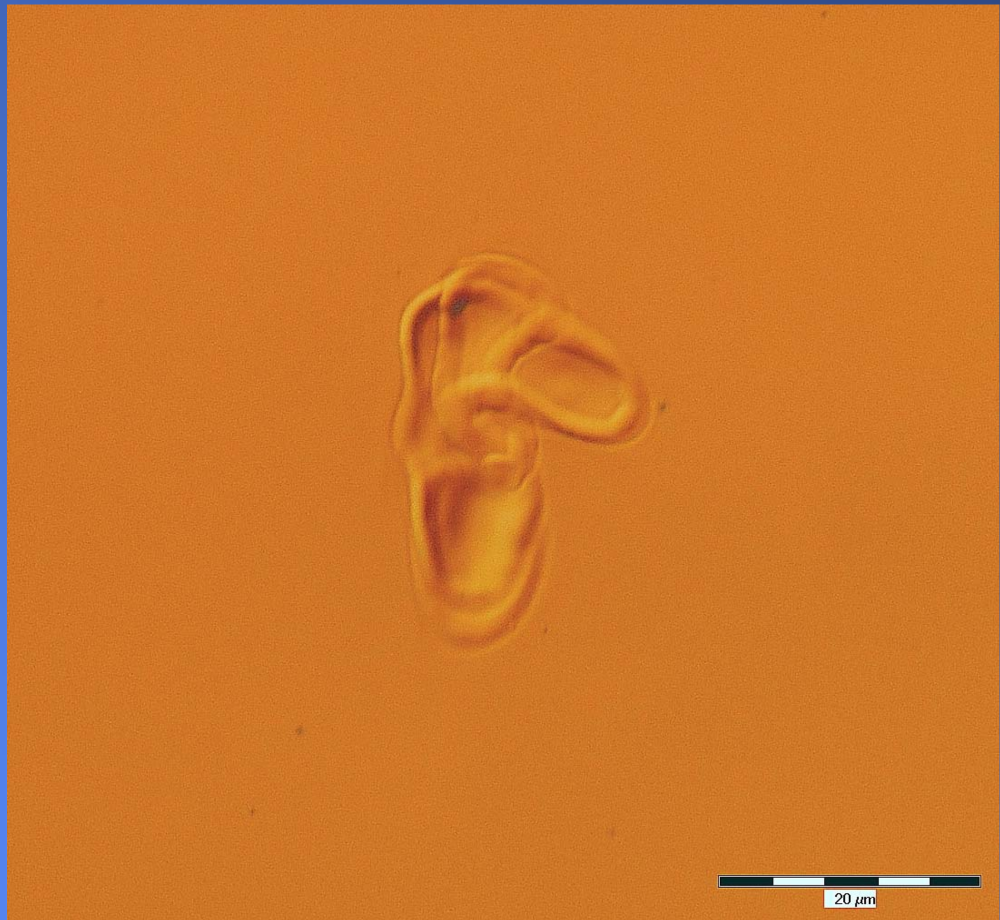

Ablation of monocrystalline silicon by a train of ten pulses of 32-nm FEL radiation (BL2 at FLASH, Fall 2005).

Three regimes can be distinguished in PMMA response to intense soft x-ray radiation

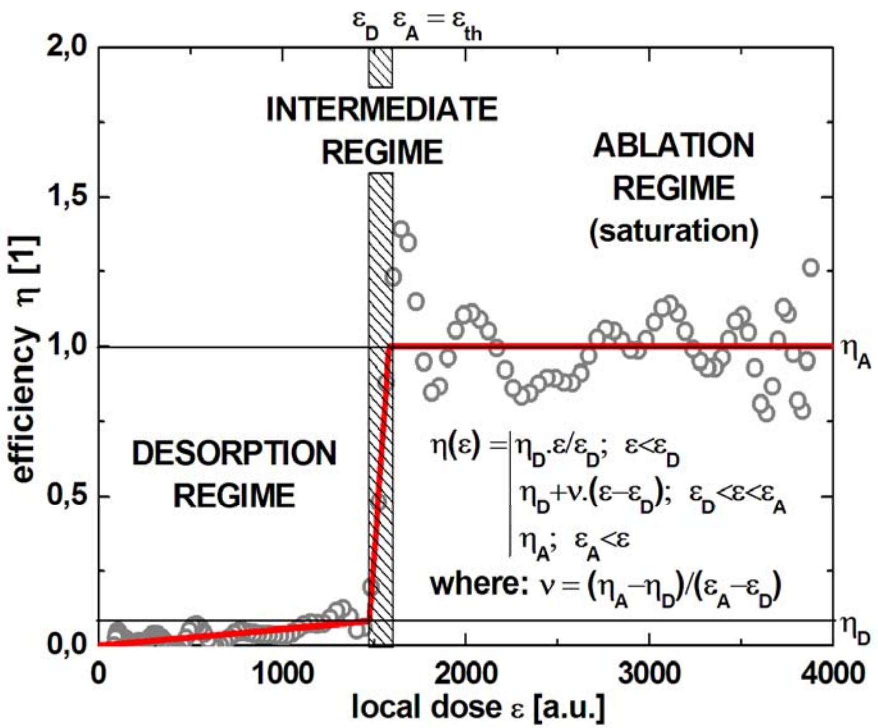

DESORPTION REGIME – below threshold process of single photon material removal occurring at beam tales and creating shallow craters (depth ~ 1nm)

INTERMEDIATE REGIME – steep rising edge of the efficiency curve. Unstable regime involving both: ablation and desorption.

ABLATION REGIME – above threshold process of collective material removal creating deep craters (depth ~ attenuation length)

$$\eta(\varepsilon) = \frac{n_R(\varepsilon)}{n}$$

Here, the material removal efficiency in a single-compound material is a ratio between dose dependent density of removed atoms and total density of atoms in unirradiated material. Red curve in the figure has a meaning of zero approach to real efficiency curve.

Single-shot damage to PMMA by focused FLASH beam

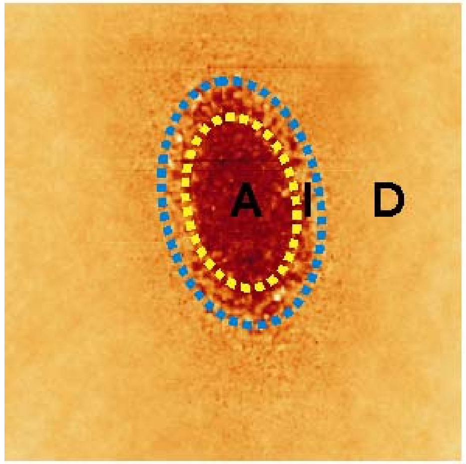

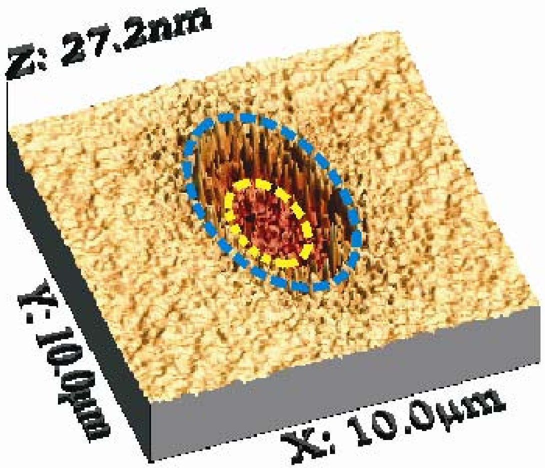

A shallow crater created by a pulse of radiation from FLASH at 21.7nm. The fluence is slightly above the threshold (~10mJ/cm^2) distinguishing the ablation, intermediate, and desorption regimes of material removal (A – the ablation region, I – the intermediate region, D – the desorption region).

A crater created by the focused beam of FLASH at 21.7nm distinguishing between ablation and desorption regimes. Blue area represents mild surface modification caused by desorption.

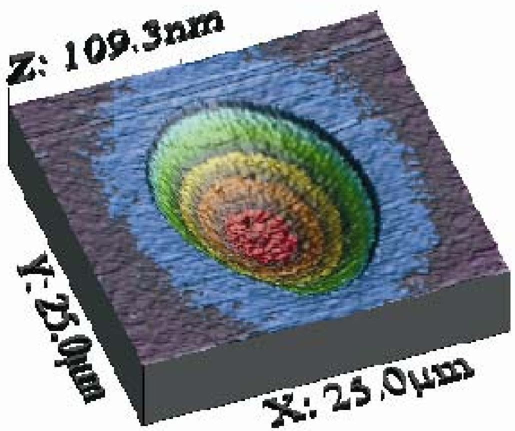

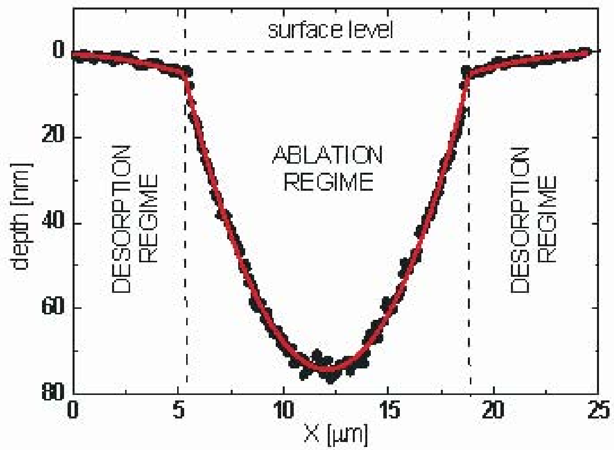

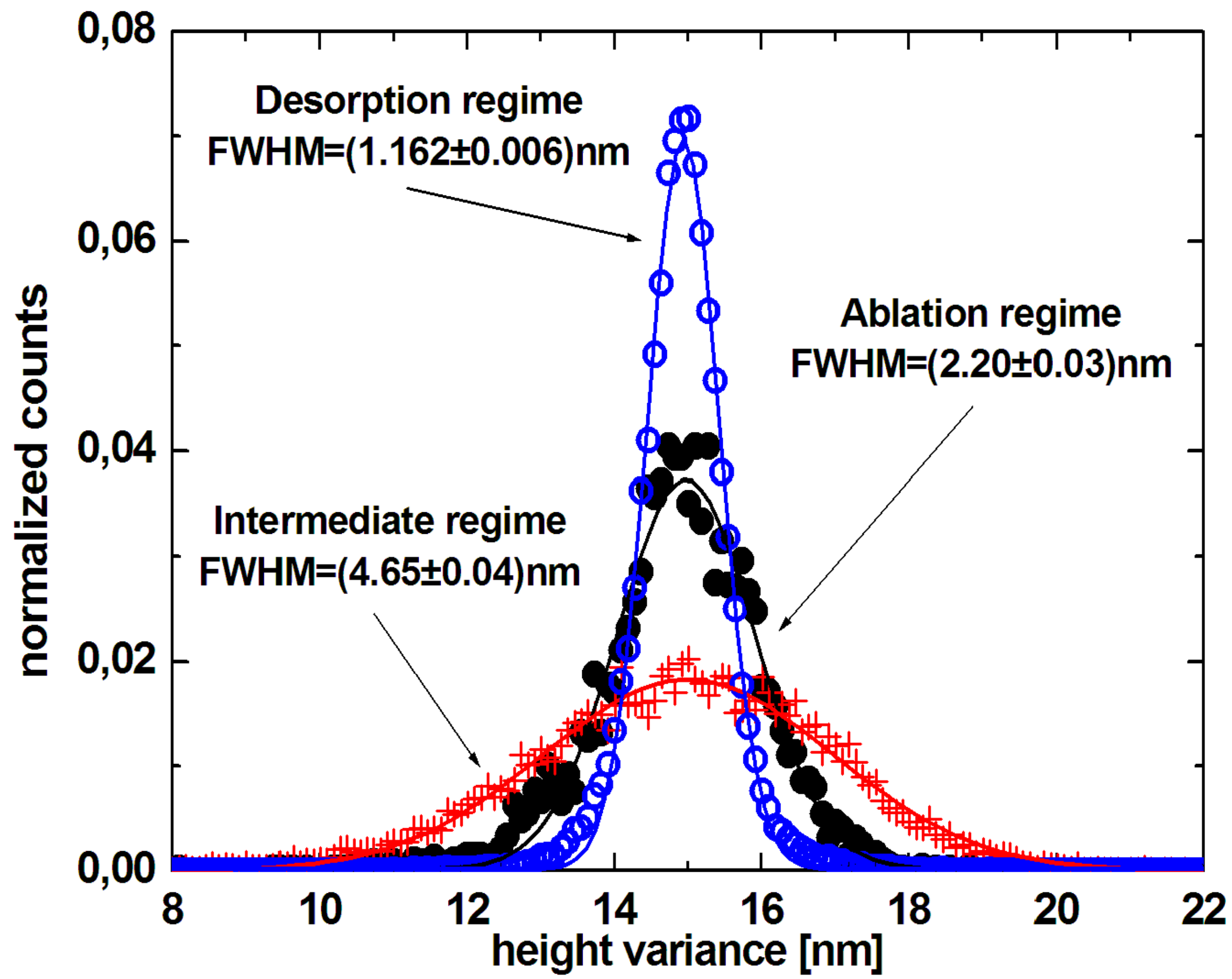

AFM surface roughness measurement for particular interaction regimes.

Desorption of PMMA

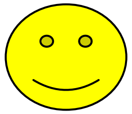

This is not a MD simulation!

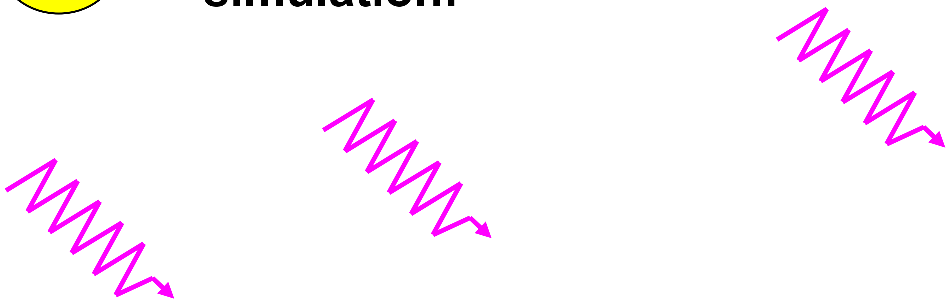

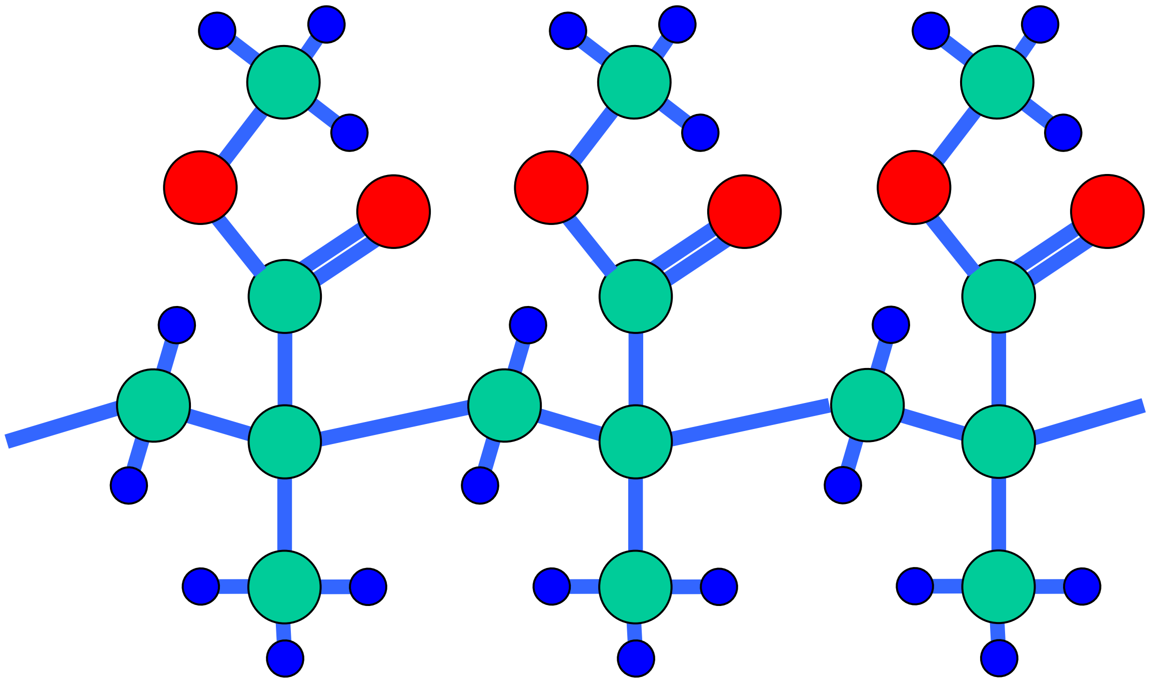

Few soft x-ray photons cannot decompose the PMMA main chain efficiently, but the probability of fragment release is not zero. Desorption of the material starts, occurring at low fluences.

Ablation of PMMA

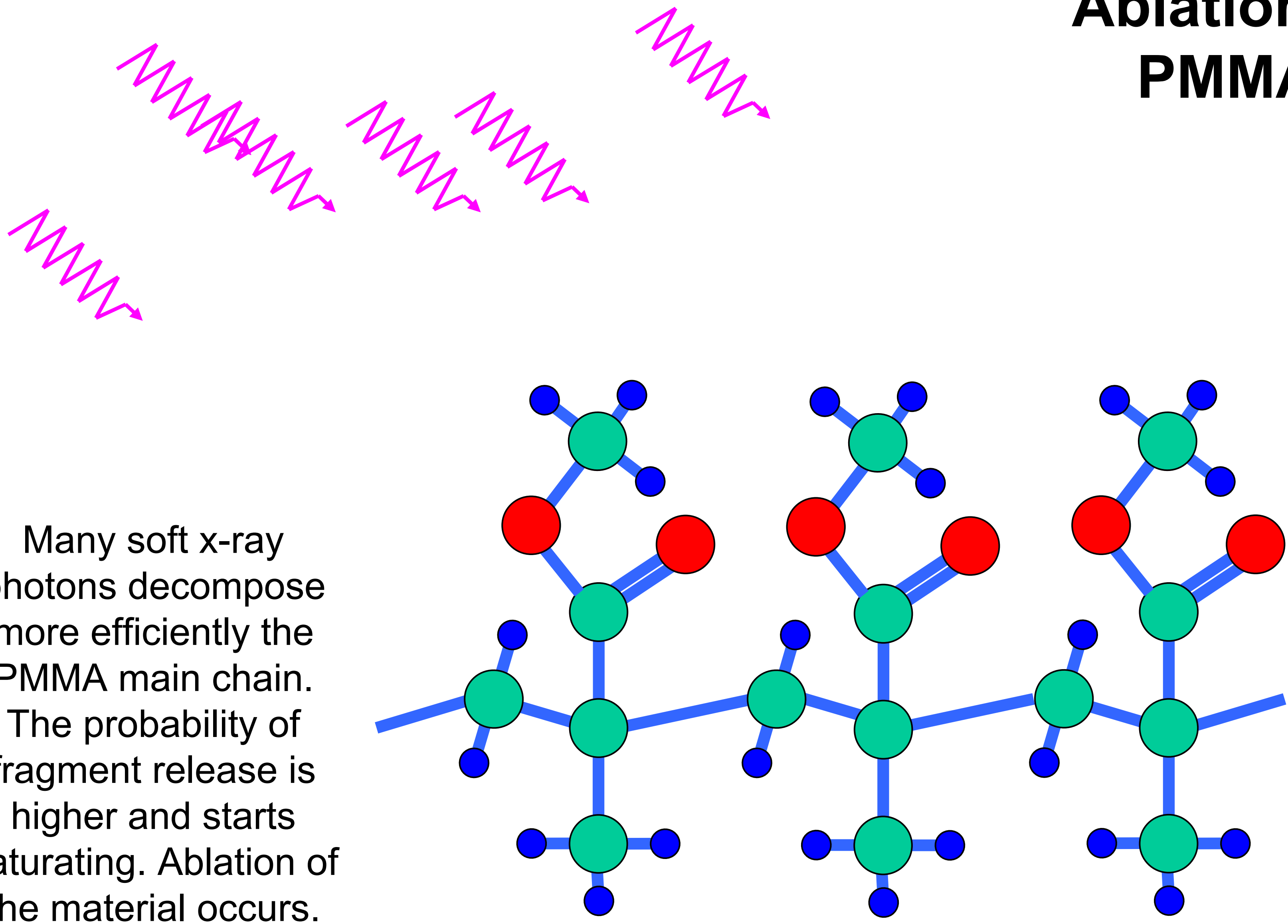

Many soft x-ray photons decompose more efficiently the PMMA main chain. The probability of fragment release is higher and starts saturating. Ablation of the material occurs.

Desorption\ablation model and crater morphology

- Let's assume the local absorbed dose in the form:

$$\varepsilon(x,y,z)=\varepsilon_0 f(x,y)e^{-z/l_{at}}$$

- Satisfying the condition of local and sudden response, i.e., neglecting any longitudinal and transverse energy transfer from irradiated region to the pristine material (charge carrier diffusion, heat conduction), we are allowed to express the crater morphology as follows:

$$d(x,y)=l_{at}\int_0^{\varepsilon_0 f(x,y)}\frac{\eta(t)}{t}\cdot dt$$

- Where:
  - •l_{at} … PMMA attenuation length
  - •ε_0 … local peak dose absorbed in the material
  - •f(x,y) … transverse intensity profile
  - •η(ε) … dose dependent material removal efficiency

Dose-dependent crater profile simulation

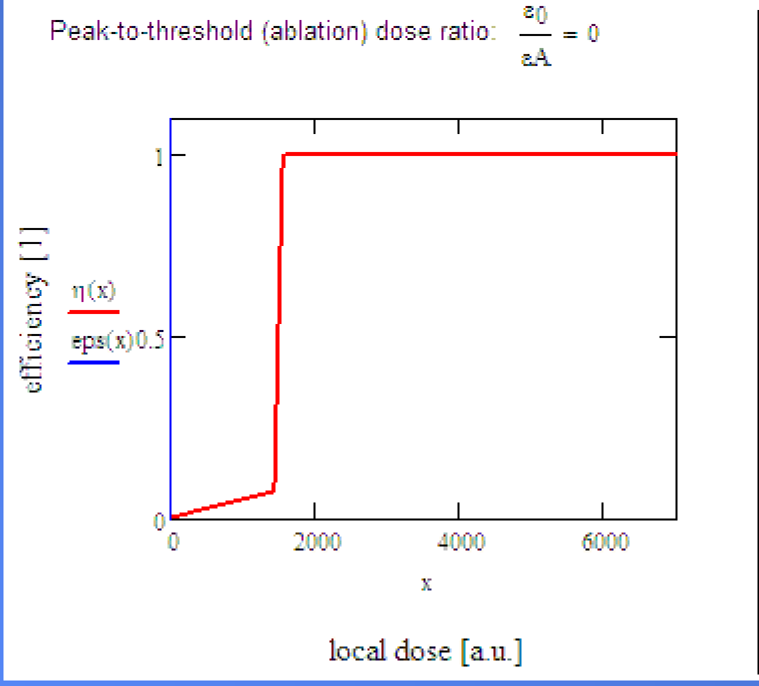

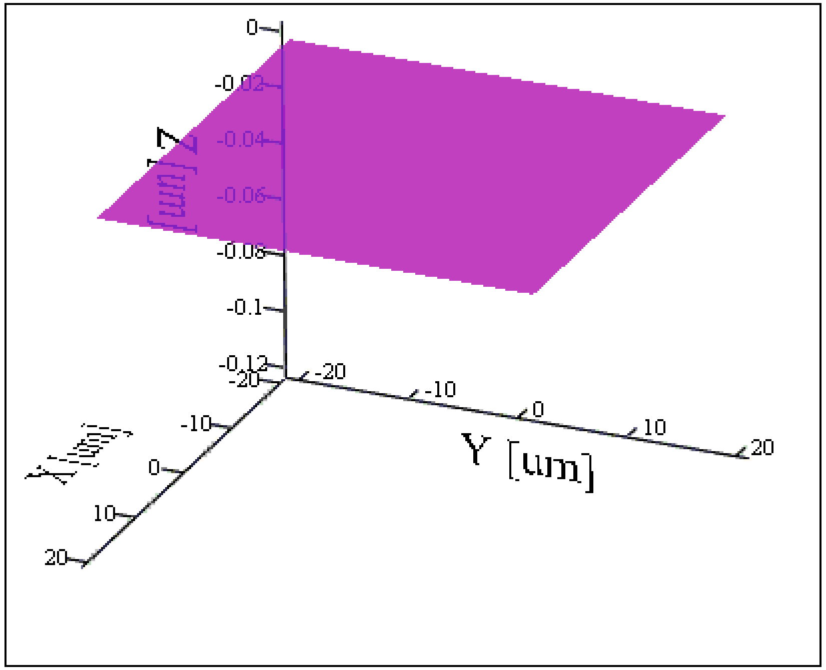

A perfect Gaussian beam profile is assumed in the simulation. Parameters of the material removal efficiency curve were taken from the measurement (η_D~0.07, η_A=1, ε_D=1460 a.u., ε_A=1580 a.u.).

Method of material removal efficiency measurement

- **Assuming a perfect Gaussian probe beam $\varepsilon(x) = \varepsilon_0 \cdot \exp(-x^2/\rho^2)$, the material removal efficiency curve is to be determined from a transverse crater cross-section measured by means of AFM as follows:**

$$\eta(\varepsilon) = -\frac{\rho^2}{2x l_{at}} \cdot d'(x) \Big|_{x=\pm\rho\sqrt{\ln(\varepsilon_0/\varepsilon)}}$$

- **Where:**
  - **x … transverse coordinate**
  - **d'(x) … first derivative of the transverse crater profile cross-section**
  - **ρ … beam radius (at 1/e of maximum)**
  - **l_{at} … attenuation length**
  - **ε_0 … peak local dose**

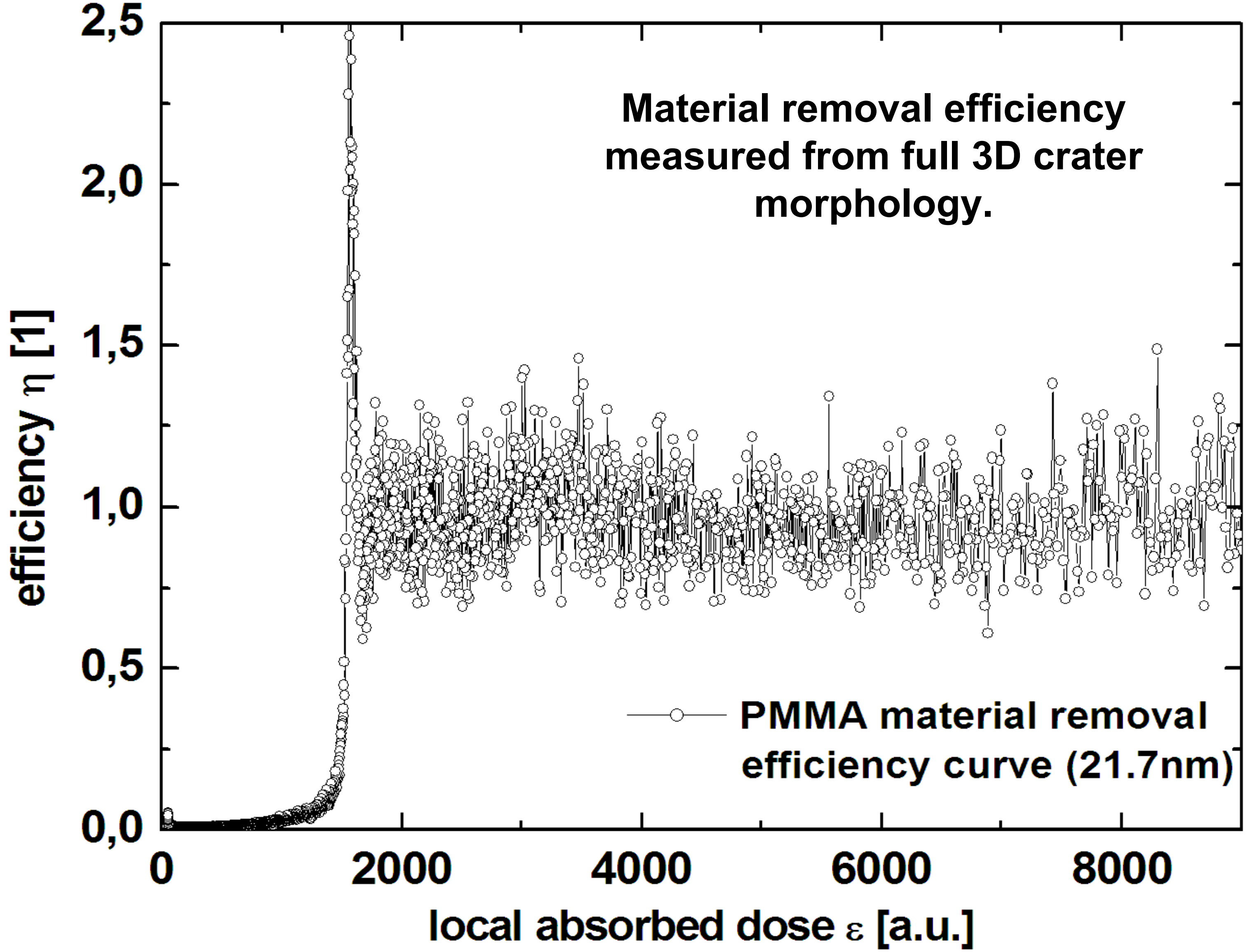

Material removal efficiency measured from full 3D crater morphology.
PMMA material removal efficiency curve (21.7nm)
efficiency η [1]
2,5
2,0
1,5
1,0
0,5
0,0
0
2000
4000
6000
8000
local absorbed dose ε [a.u.]

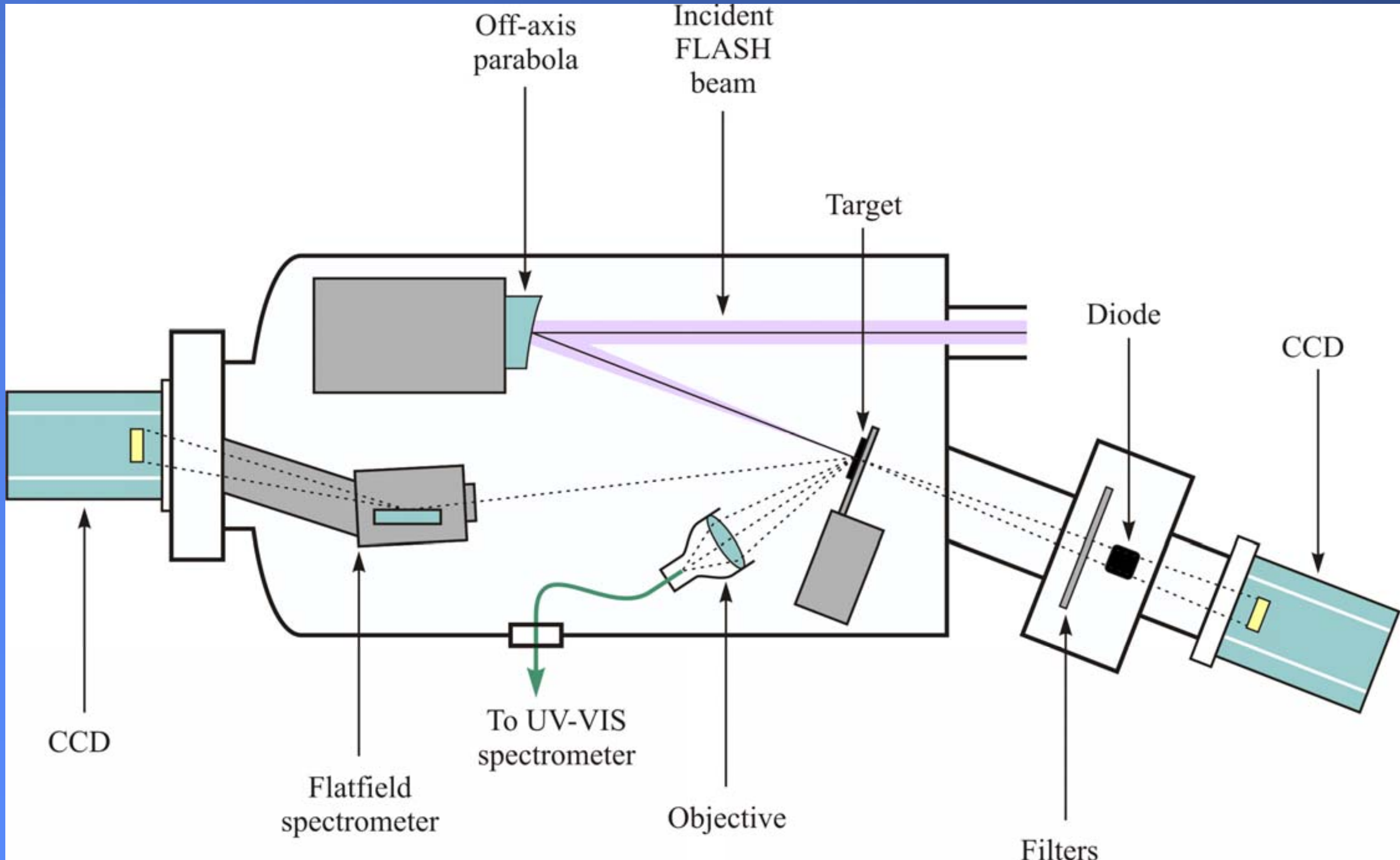

Experimental layout of the A/T measurement using microfocusing 13.7-nm FEL radiation by off-axis parabolic mirror (OAP)

Micro-focusing 13.7-nm FLASH beam by OAP

simulation:
h.e. 0.3 nm;
FWHM =
= 300nm

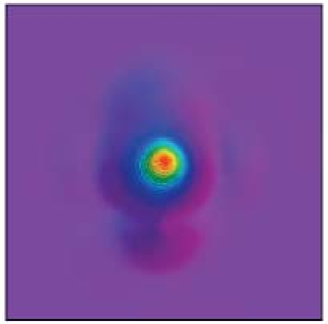

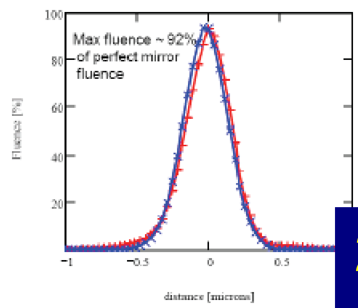

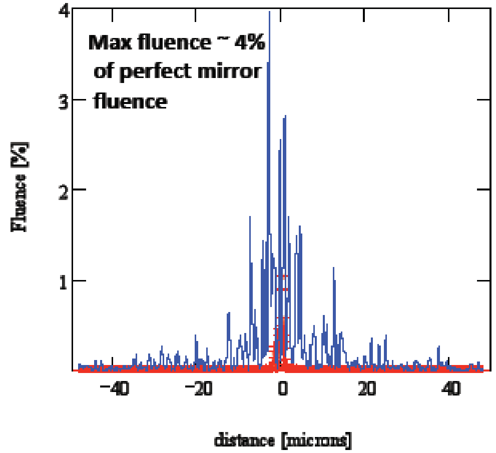

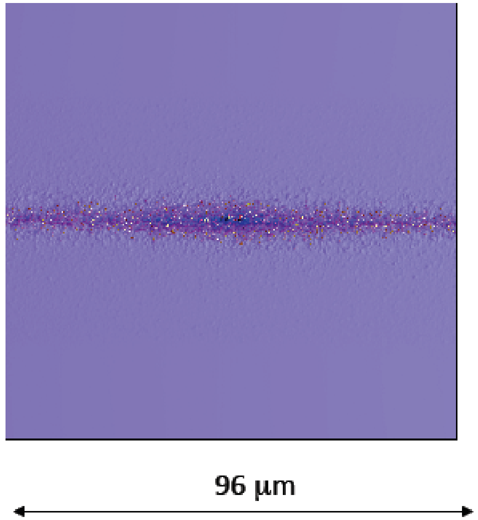

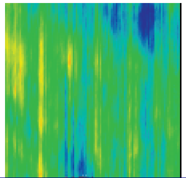

Surface height error map 1x1 cm
(Zygo interferometer)
Height error 1.6 nm rms

2007

2008: S. Bajt, A. Nelson, J. Krzywinski + LBL, LLNL, DESY, CL [*Opt. Express* **17**, 18271 (2009)]

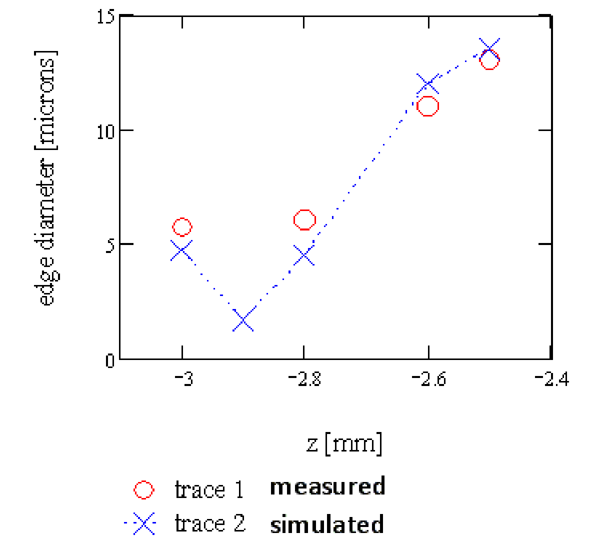

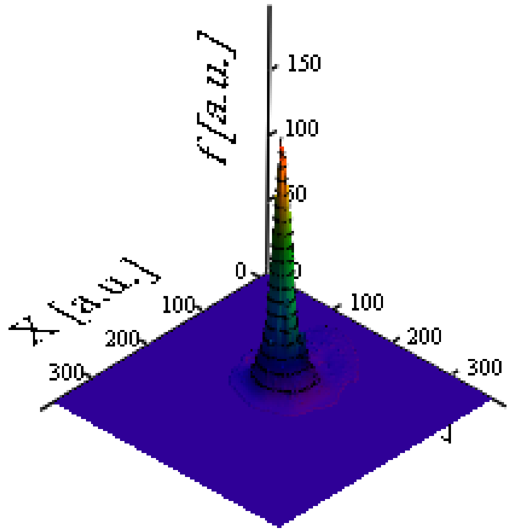

$P=F_0/F_{th}$	194,4
Q	0,87 µm^2
$S_{1/e}$	0,482 µm^2
S_{FWHM}	0,326 µm^2
D_Q	1,05 µm
$D_{1/e}$	0,784 µm
FWHM	0,644 µm

Ablation imprints of the focused beam

- **Transverse beam profile reconstruction**
  - soft x-ray beam profile reconstruction utilizing ablative imprints in PMMA (poly(methyl metacrylate) to derive transverse irradiance distribution
  - the ablation imprint's morphology is investigated by means of the atomic force microscopy (AFM)
- **Model assumptions and conditions:**
  - non-thermal ablation (no thermal melting)
  - Lambert-Beer law of radiation absorption
  - local energy deposition (no transverse heat or charge transfer)
  - attenuation length << Rayleigh range
  - irradiance-independent ablation threshold

$$f(x,y) = \frac{F_{th}}{F_0} \exp\left(\frac{d(x,y)}{l_{at}} \right)$$

Where:

$f(x,y)$ … reconstructed beam profile

$d(x,y)$ … measured crater profile

F_{th} … threshold fluence

F_0 … peak fluence

l_{at} … attenuation length

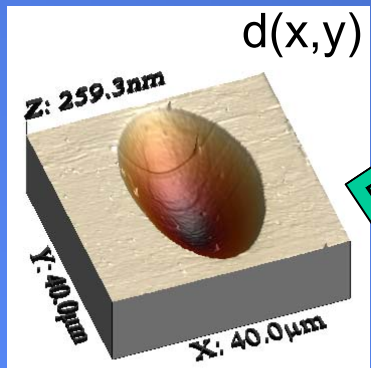

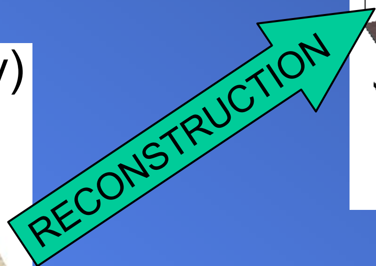

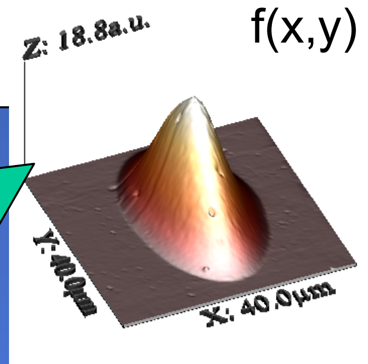

Chalupsky et al., *Opt. Express* **15**, 6036 (2007).

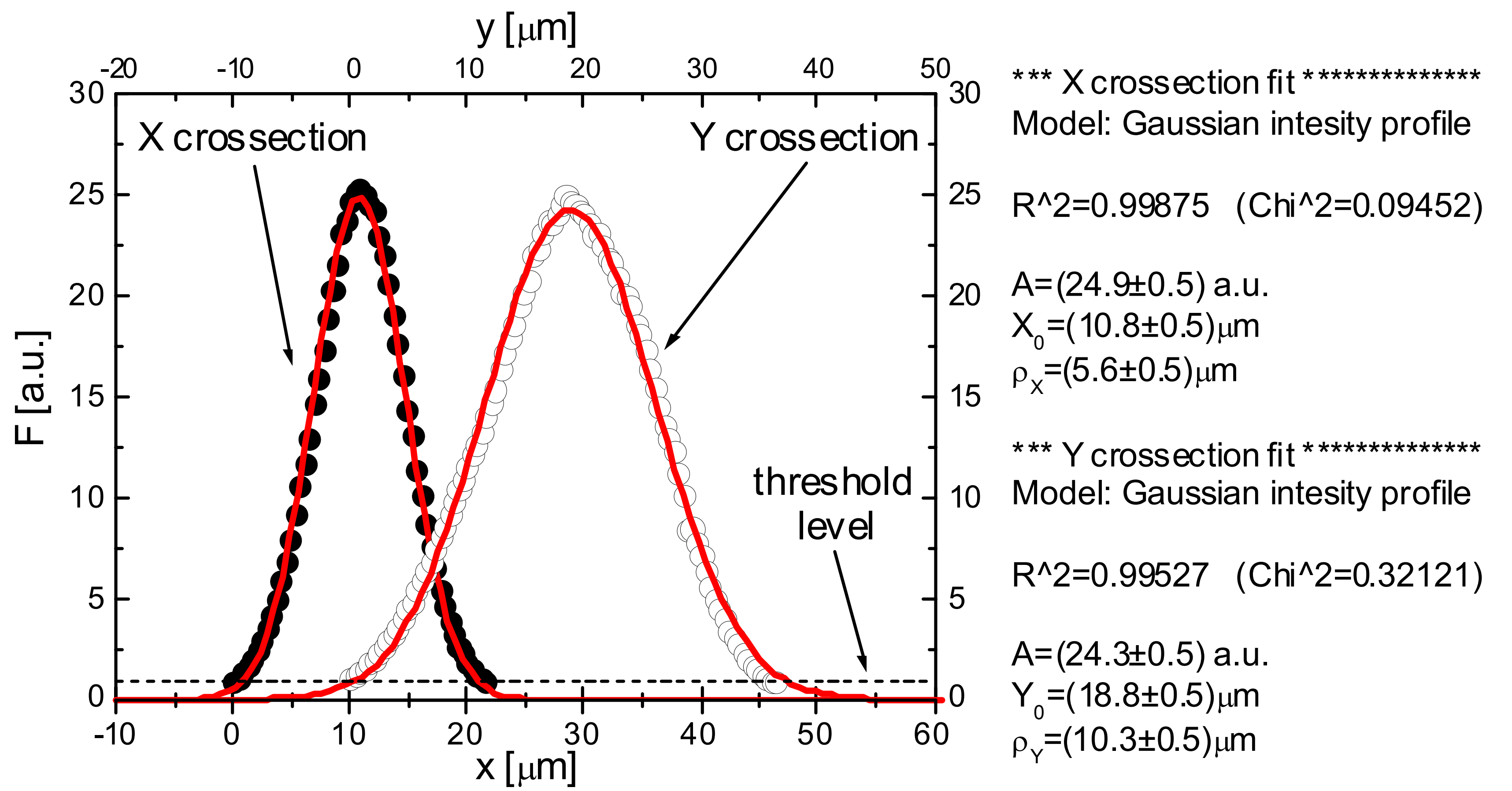

J. Chalupsky et al.: *Opt. Express* **15**, 6036 (2007).

- **Advantages:**
  - direct “in focus” detector (no propagation algorithms needed)
  - almost AFM-like resolution
- **Disadvantages:**
  - dynamic range limited by non-thermal and thermal ablation threshold
  - “ex situ” detector
  - limited wavelength range (surface RMS enhancing with the photon energy)

- **Solution:** high-Z materials (lead tungstate – $PbWO_4$)

Reliable range

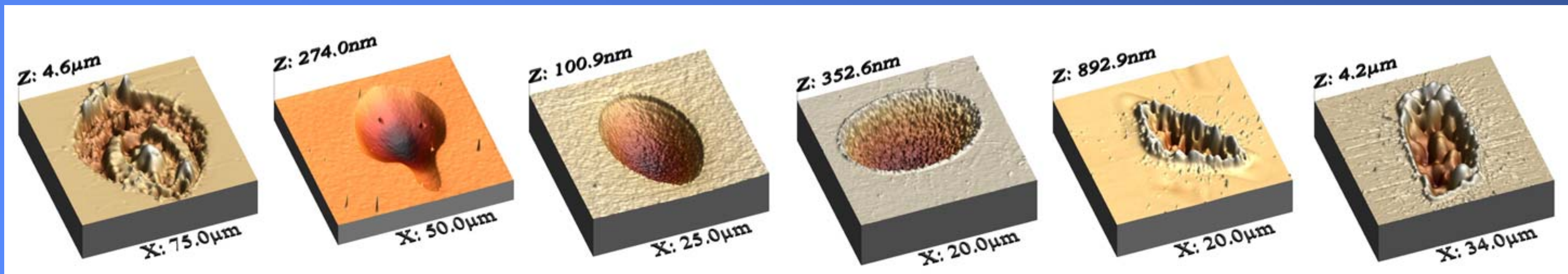

800nm	**32nm**	**21.7nm**	**13.5nm**	**7.1nm**	**1.49nm**
1.55eV	**38.7eV**	**57eV**	**91.7eV**	**174.3eV**	**830eV**

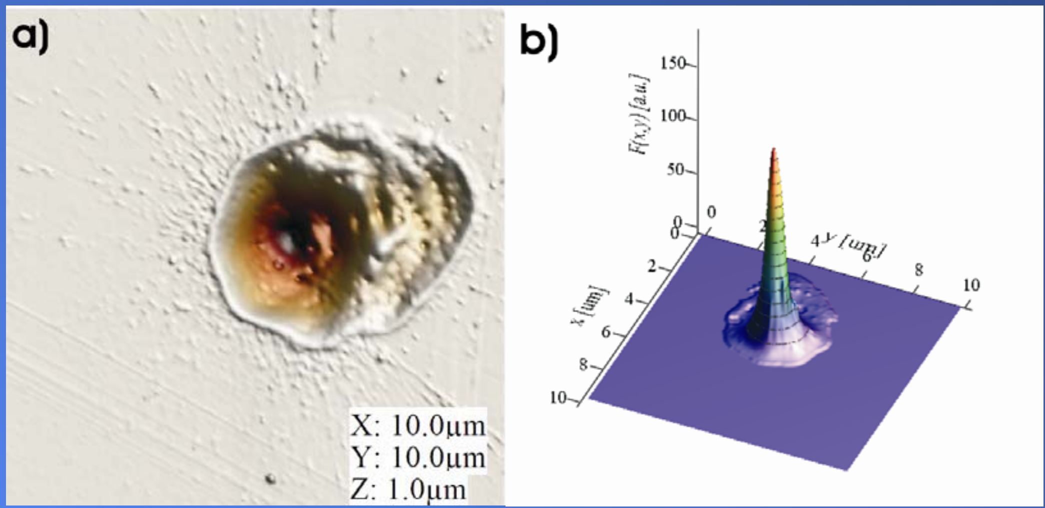

A.J. Nelson et al., *Opt. Express* **17**, 18271 (2009)

An example of transverse beam profile reconstruction exploiting ablative imprints in PMMA. A sub-micron focus at 13.5nm has been achieved and characterized at FLASH.

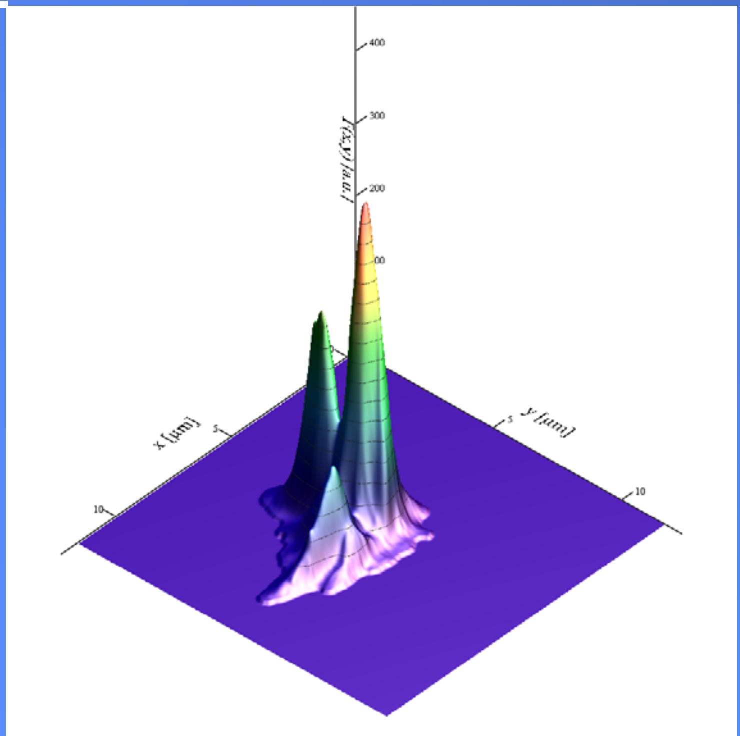

Quiz question: What is the full width at half maximum (FWHM) of this beam profile?

Answer: FWHM is a bit misleading used for characterizing non-Gaussian beams.

Solution: Define the effective beam diameter.

F-scan technique

- fluence scan (F-scan) method = measurement of the beam cross-section area at various fluence levels
- derived from the beam profile reconstruction eq. for the surface contour:

$$f(x,y) = \frac{F_{th}}{F_0} \exp\left(\frac{d(x,y)}{l_{at}}\right) \xrightarrow{d(x,y)=0} f(x,y) = \frac{F_{th}}{F_0} = \frac{1}{p}$$

- the surface contour represents a beam contour at level 1/p of maximum
- varying the peak fluence F_0, i.e. the peak-to-threshold fluence ratio p, we scan through the beam profile

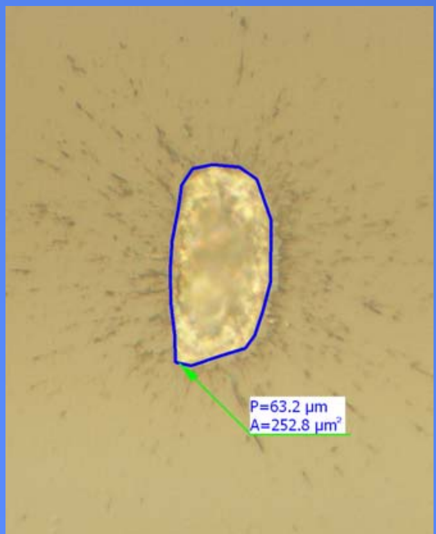

An AFM scan (on the right) and Nomarski image (on the left) of an ablative imprint in PMMA created by 15-Å (830eV) LCLS radiation 26mm out of the focus (AMO station). Even though the surface roughness is increased, the surface contour remains preserved.

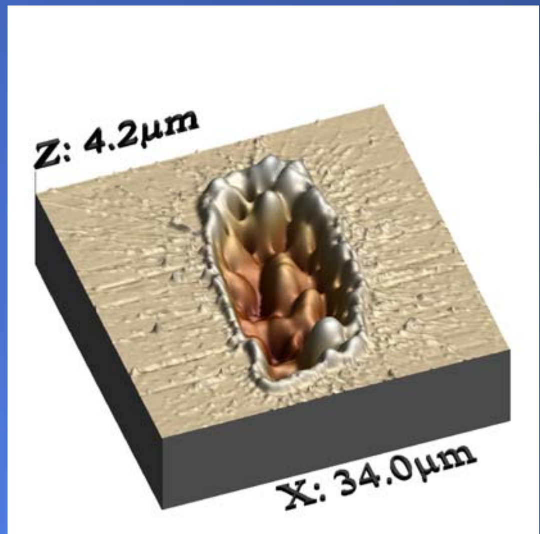

J. Chalupsky et al.: *Opt. Express* **18**, 27836 (2010).

(i) advantages:

- the f-scan method enhances the dynamic and wavelength range of the ablative imprints methods by several orders of magnitude
- does not need AFM measurements
- very high resolution
- applicable to any material with an irradiance-independent ablation threshold
- good tool to characterize non-Gaussian beams

(ii) difficulties:

- needs a stable beam profile; shot-to-shot fluctuations must be minimized
- not suitable for heavily attenuated beams (limited by the ablation threshold)
- high-irradiance imprints may be influenced by piston effect and spallation

Why could be the high resolution of use?

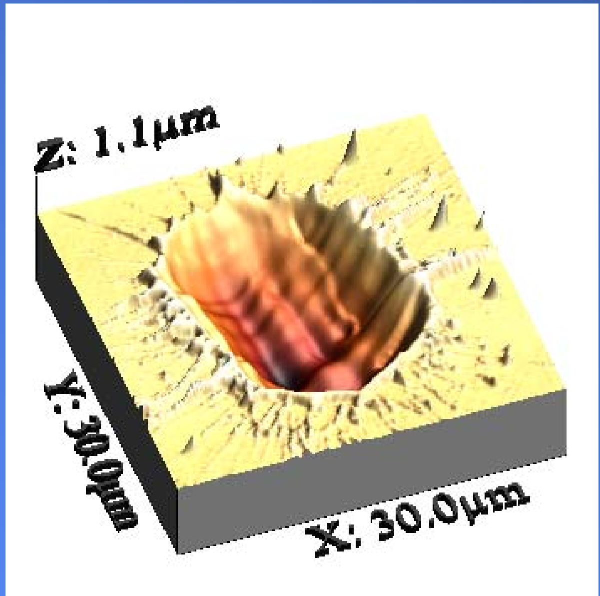

- an ablative imprint in $PbWO_4$ created by 6Å LCLS radiation (2keV) out of the focus

- the pulse energy adjusted by a gas attenuator (T=1%)

- no Be filters used

- in principle usable for beam profile reconstruction at 2keV

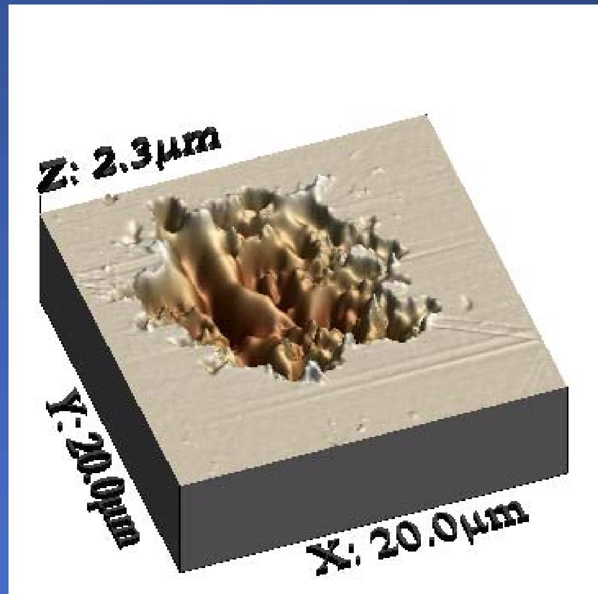

- an ablative imprint in $PbWO_4$ created by 6Å LCLS radiation (2keV) out of the focus

- the pulse energy adjusted by a gas attenuator (T=2%)

- Be filters used (T=20%)

- a micron-sized speckle structure observed indicating the wavefront has been shattered by the Be filter

Effective beam area (A_{eff})

- is to be regarded as a reference quantity for all spot-size definitions (4σ, RMS, FWHM,…)
- provides mathematically correct relation between the pulse energy (E) and peak fluence (F_0)
- best approach to treat non-Gaussian beams
- measurable by means of the F-scan

Exercise $\rightarrow$ define: $F(x,y) = F_0 f(x,y)$, where: $0 \le f(x,y) \le 1$ for $(x,y) \in R^2$

$$\text{integrate: } E_{pulse} = F_0 \int_{-\infty}^{\infty}\int_{-\infty}^{\infty} f(x,y)\,dxdy = F_0 A_{eff}$$

$$\text{effective beam area: } A_{eff} = \int_{-\infty}^{\infty}\int_{-\infty}^{\infty} f(x,y)\,dxdy$$

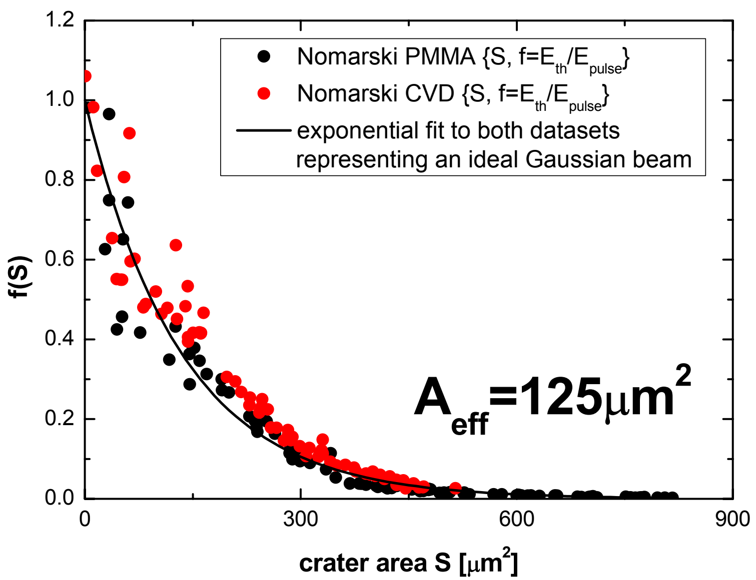

The threshold-to-peak fluence ratio $f = 1/p = E_{th}/E_{pulse} = F_{th}/F_0$ as a function of the surface contour area S. PMMA and CVD diamond (chemical vapor deposition) samples were both irradiated at the same position by focused LCLS beam (830 eV, AMO station). The effective area is represented by the area below the measured curves.

Longitudinal beam profile characterization

- **Stigmatic beams**
  - the shape of the ablative imprints an their dependence on the longitudinal z-position provide information about the focusing performance
  - **assuming** a stigmatic Gaussian beam we may express the crater area (surface contour area) as:

$$S\left(z,F_0\right)=S_{foc}\left(1+\frac{\left(z-z_c\right)^2}{z_0^2}\right)\left(\ln\frac{F_0}{F_{th}}-\ln\left(1+\frac{\left(z-z_c\right)^2}{z_0^2}\right)\right)$$

Where:

S_{foc} … focal spot area

z_c … beam waist position

z_0 … Rayleigh range

F_{th} … threshold fluence

F_0 … peak fluence

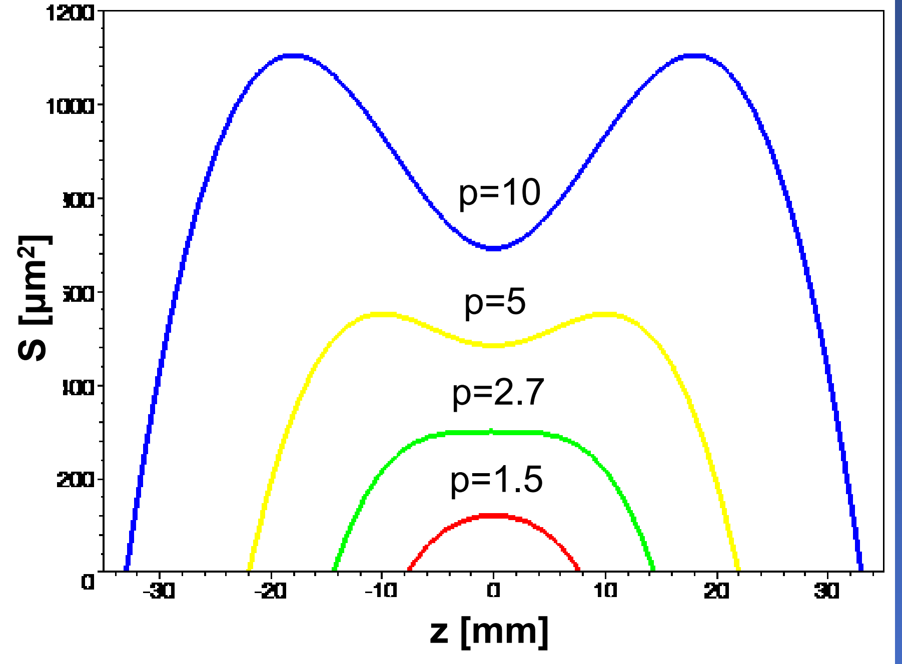

Theoretical dependence of the crater area on the longitudinal z-position at various peak-to-threshold fluence ratios (S_{foc}=300µm^2,z_0=11mm,z_c=0mm).

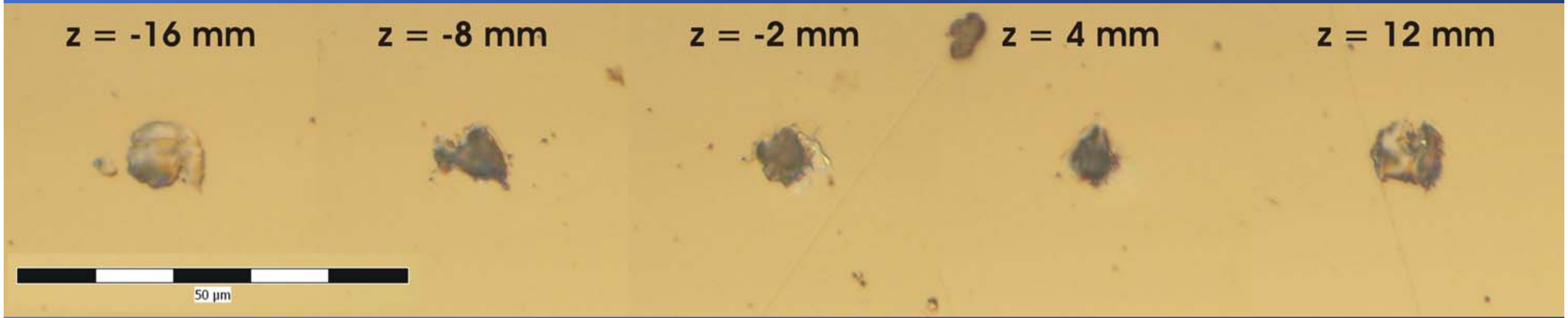

Almost circular ablative imprints in $PbWO_4$ created by a stigmatic focused LCLS beam at 1600 eV (SXR station, perfectly aligned K-B optics, non-monochromatized "white" beam).

Measured crater areas in relation to the longitudinal z-position. Bars, circles, and triangles represent different attenuation levels. The data are fitted by the stigmatic Gaussian model function.

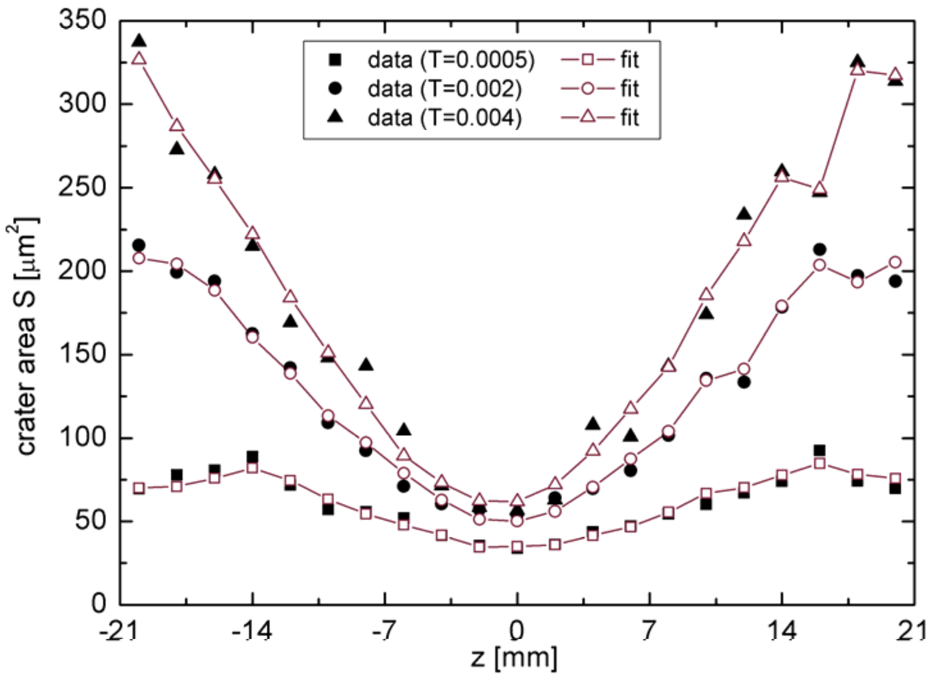

- **Astigmatic beams**
  - an astigmatic beam is usually responsible for elliptical imprints
  - the orientation of the major axis changes by 90 degrees when scanning through the focus
  - from the fit of a theoretical Gaussian model we may judge about the astigmatism
  - **assuming** an astigmatic Gaussian beam we may express the crater radii as:

$$r_1(z,F_0)=\rho_1(z)\left(\ln\frac{F_0}{F_{th}}-\ln\left(\frac{\rho_1(z)\rho_2(z)}{\rho_{01}\rho_{02}}\right)\right)^{1/2},where:\rho_1(z)=\rho_{01}\left(1+\frac{(z-z_{c1})^2}{z_{01}^2}\right)^{1/2}$$

$$r_2(z,F_0)=\rho_2(z)\left(\ln\frac{F_0}{F_{th}}-\ln\left(\frac{\rho_1(z)\rho_2(z)}{\rho_{01}\rho_{02}}\right)\right)^{1/2},where:\rho_2(z)=\rho_{02}\left(1+\frac{(z-z_{c2})^2}{z_{02}^2}\right)^{1/2}$$

Where:

ρ_{01}, ρ_{02} … beam waist radii

z_{c1}, z_{c2} … beam waist positions

z_{01}, z_{02} … Rayleigh ranges

F_{th} … threshold fluence

F_0 … peak fluence

$\rho_1(z)$, $\rho_2(z)$ … beam radii at arbitrary z-position

Subscripts 1,2 denote sagittal and tangential plane, respectively.

Mutually coupled equations → must be fitted simultaneously.

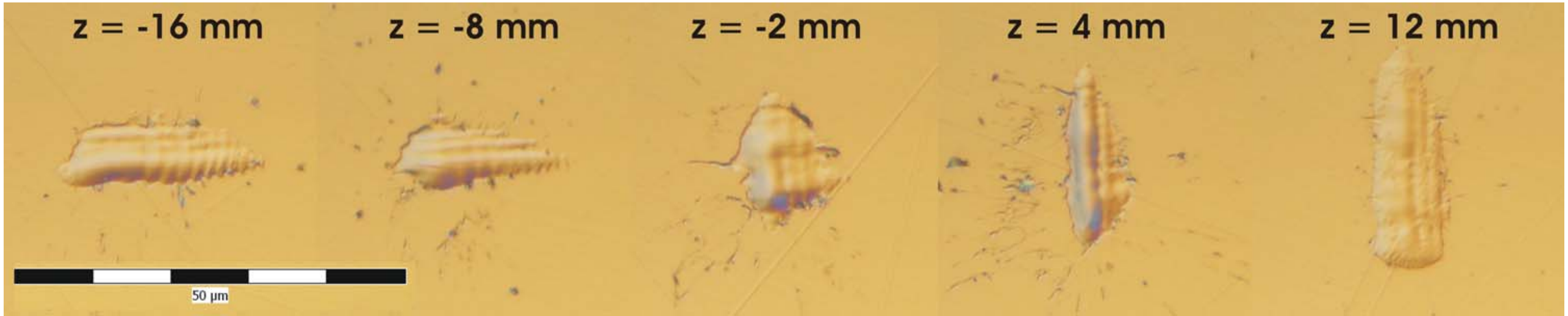

Almost elliptical ablative imprints in $PbWO_4$ created by an astigmatic focused LCLS beam at 800 eV (SXR station, misaligned K-B optics, non-monochromatized beam).

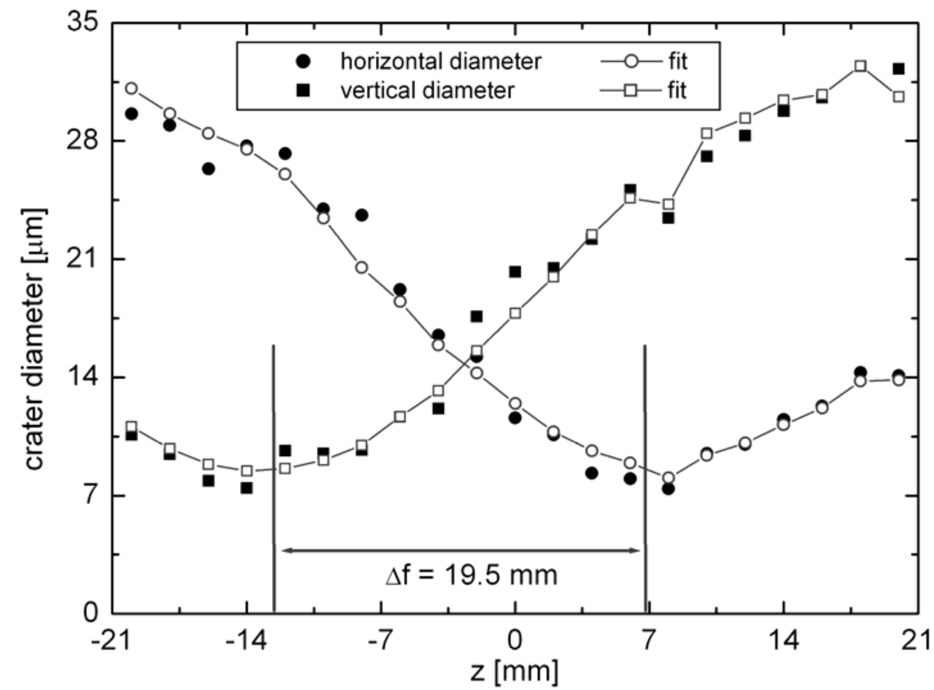

Measured horizontal and vertical crater diameters in relation to the longitudinal z-position. The data were fitted by the astigmatic Gaussian model functions in order to determine the astigmatic difference Δf, i.e., the distance between the horizontal and vertical focus.

M_h^2 = (3.6±0.5) and M_v^2 = (3.2±0.5)

Challenges for future - multi-shot desorption imprints in PMMA

- below-threshold material removal (desorption)
- multiple shots needed to modify the surface significantly
- the beam profile is proportional to the crater morphology

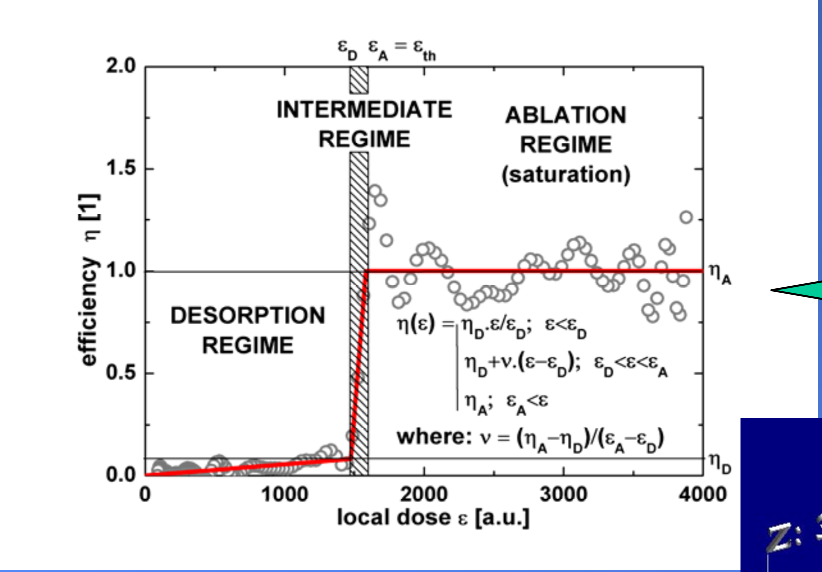

Material removal efficiency curve.
J. Chalupsky et al., *Opt. Express* **17**, 208-217 (2009)

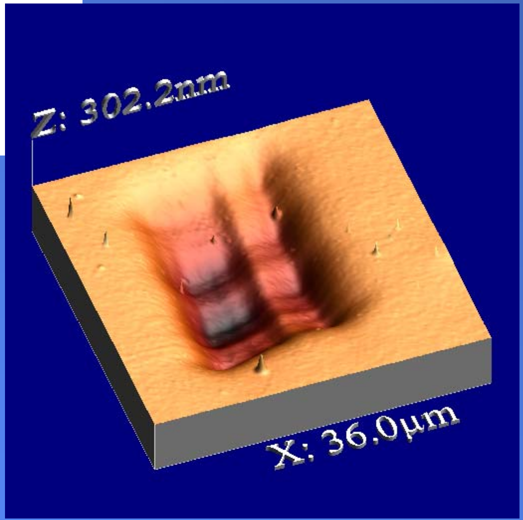

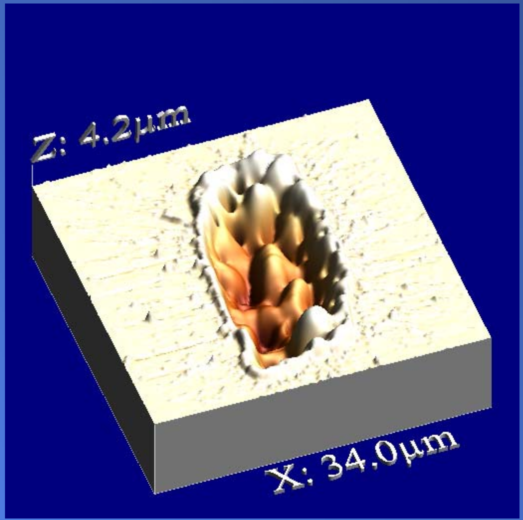

A multi-shot (300 shots) below-threshold desorption imprint (left) and a single-shot ablation (right) imprint created by focused LCLS radiation at 830eV (AMO station).

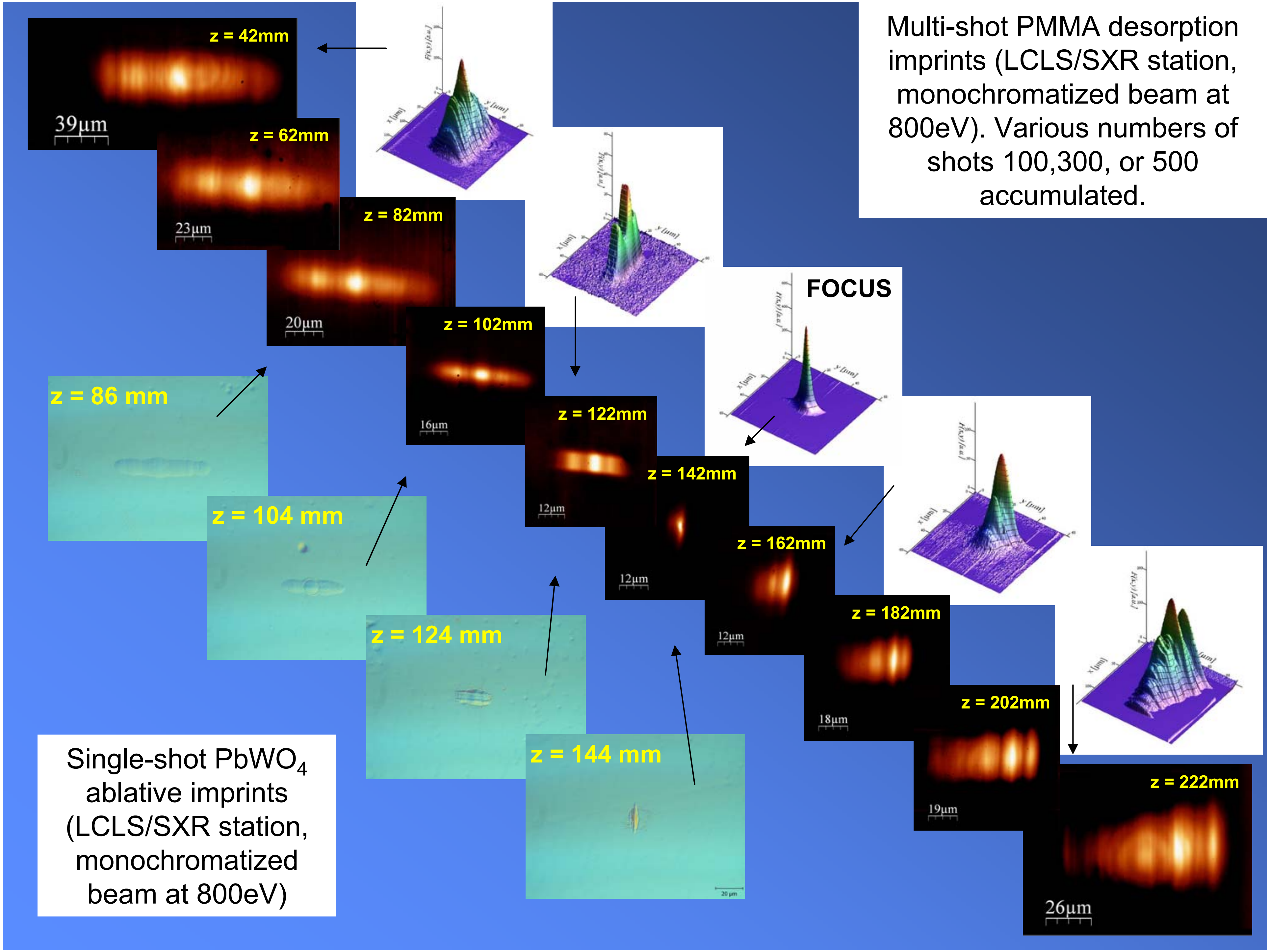
Multi-shot PMMA desorption imprints (LCLS/SXR station, monochromatized beam at 800eV). Various numbers of shots 100,300, or 500 accumulated.
z = 42mm
39µm
z = 62mm
23µm
z = 82mm
20µm
z = 102mm
16µm
z = 122mm
12µm
z = 142mm
12µm
z = 162mm
12µm
z = 182mm
18µm
z = 202mm
19µm
z = 222mm
26µm
FOCUS
z = 86 mm
z = 104 mm
z = 124 mm
z = 144 mm
Single-shot $PbWO_4$ ablative imprints (LCLS/SXR station, monochromatized beam at 800eV)

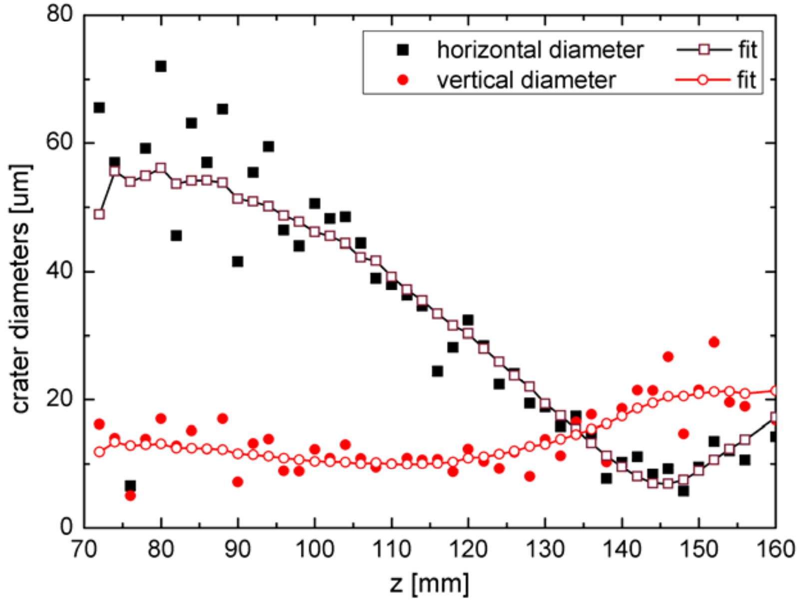

Measured crater diameters (single-shots in $PbWO_4$) fitted by astigmatic Gaussian model functions (LCLS/SXR station, monochromatized beam at 800ev).

An approximate caustic curve determined from the $PbWO_4$ measurements (geometrically averaged radii) compared to effective beam radii measured by means of multi-shot desorption imprints in PMMA. The results are in a good agreement.

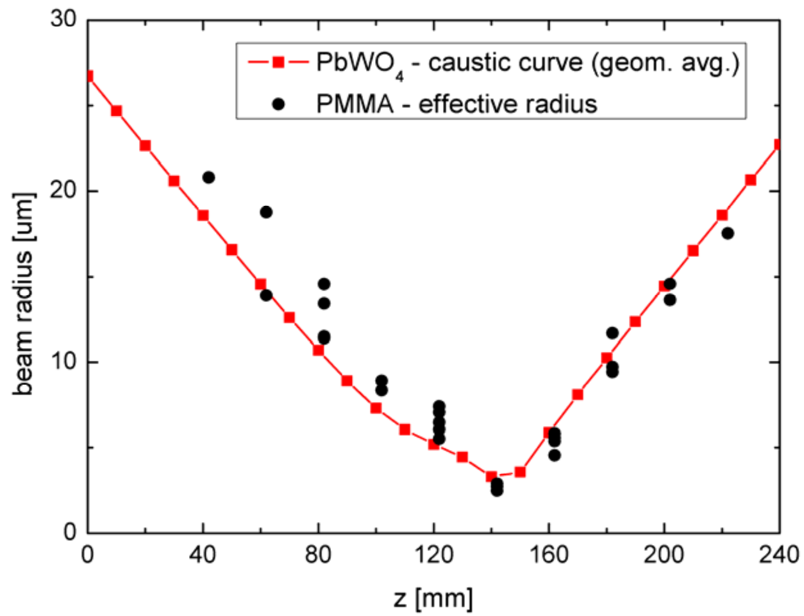

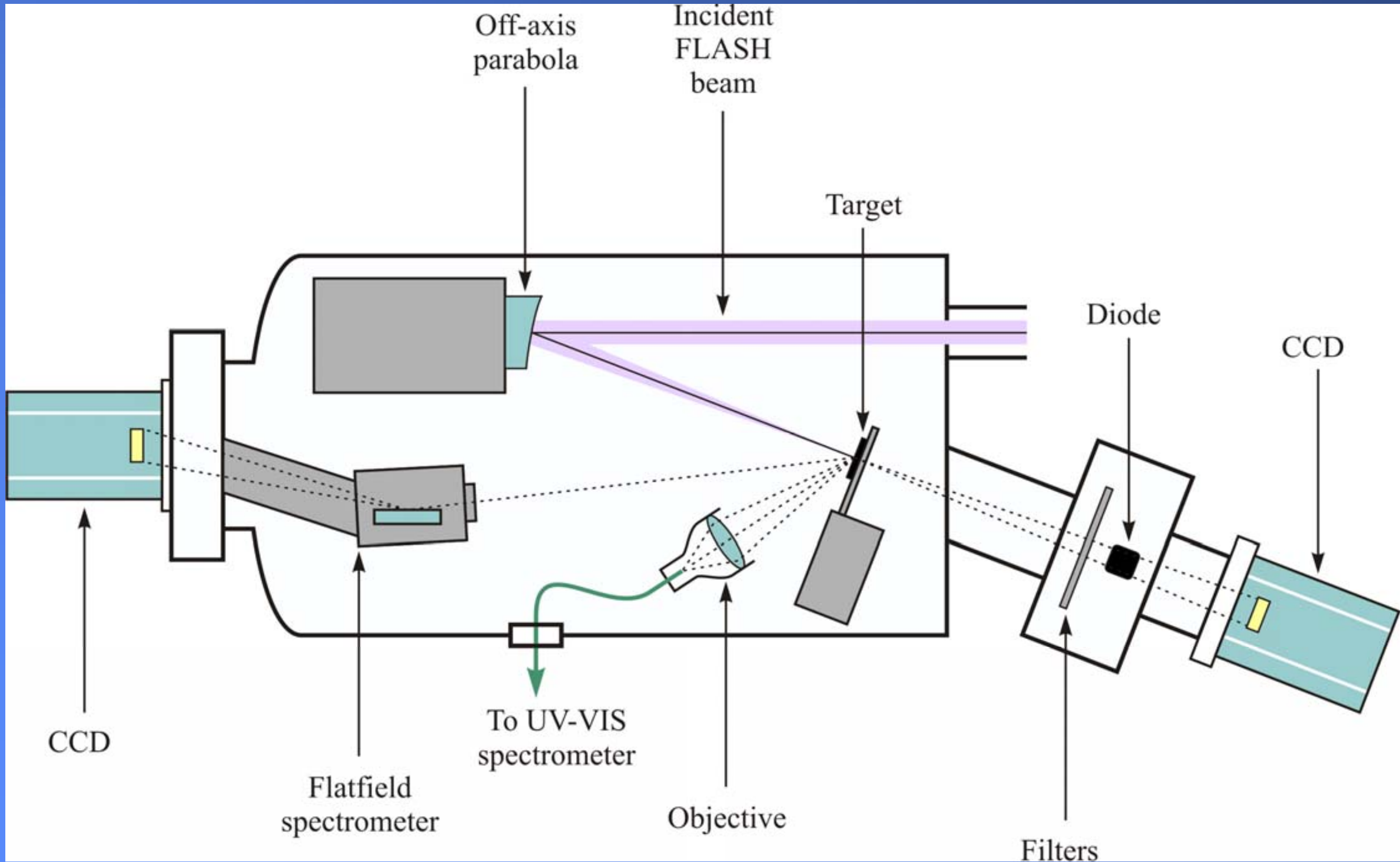

experimental layout of the A/T measurement using microfocusing 13.7-nm FEL radiation by off-axis parabolic mirror (OAP)

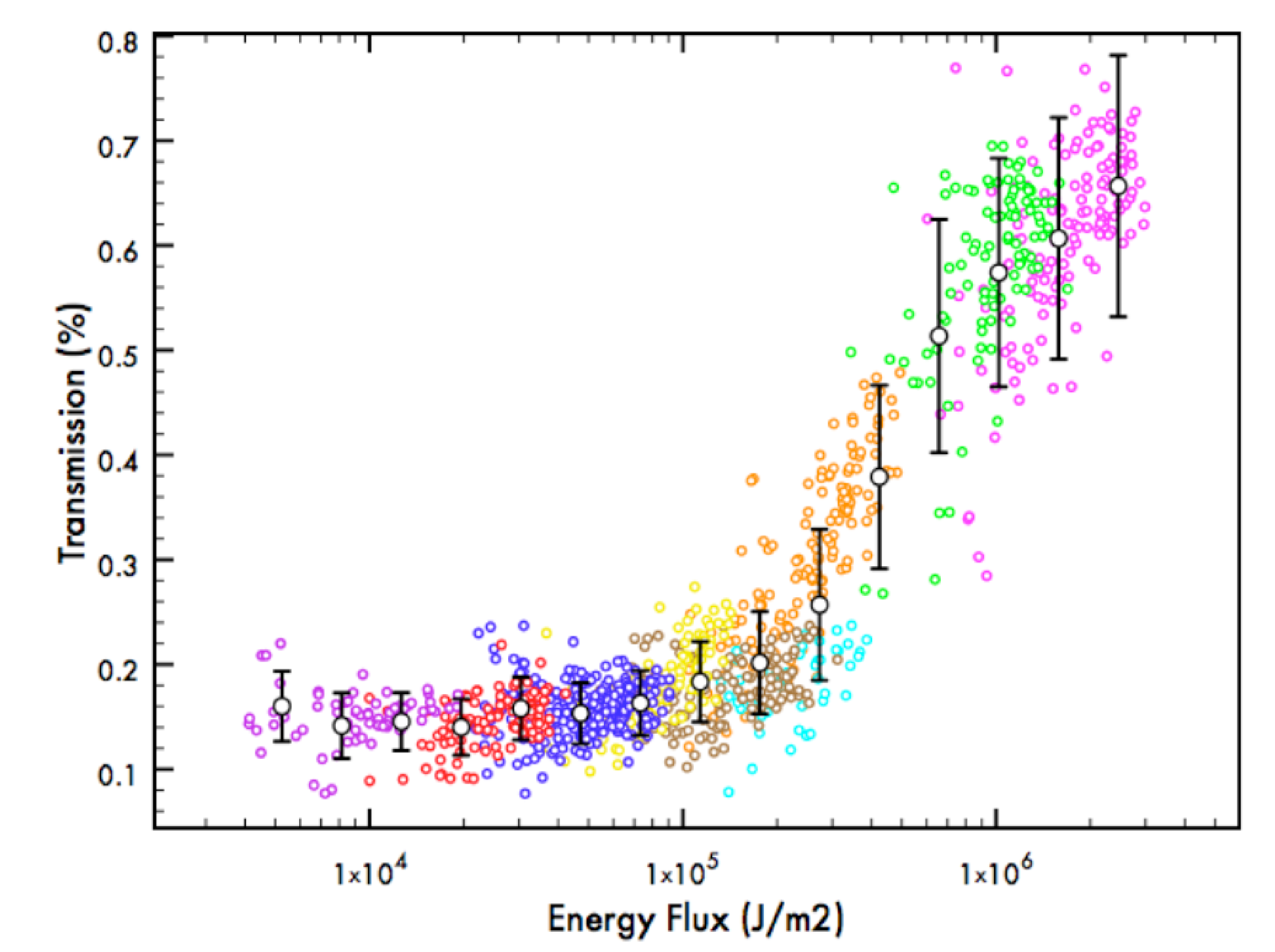

NANOSCOPY LAB IP-ASCR-Prague

Transmission of 52-nm Al foil (10-nm Al_2O_3) for the 13.7-nm FLASH beam focused by Si/Mo coated OAP at an irradiance ranging from 10^{14} W/cm^2 to 10^{17} W/cm^2 [B. Nagler a kol.: Turning solid aluminium transparent by intense soft X-ray photo-ionization, *Nature Physics* 5, 693 (2009)]

electronic structure of solid Al (L shell)

NANOSCOPY LAB
IP-ASCR-Prague

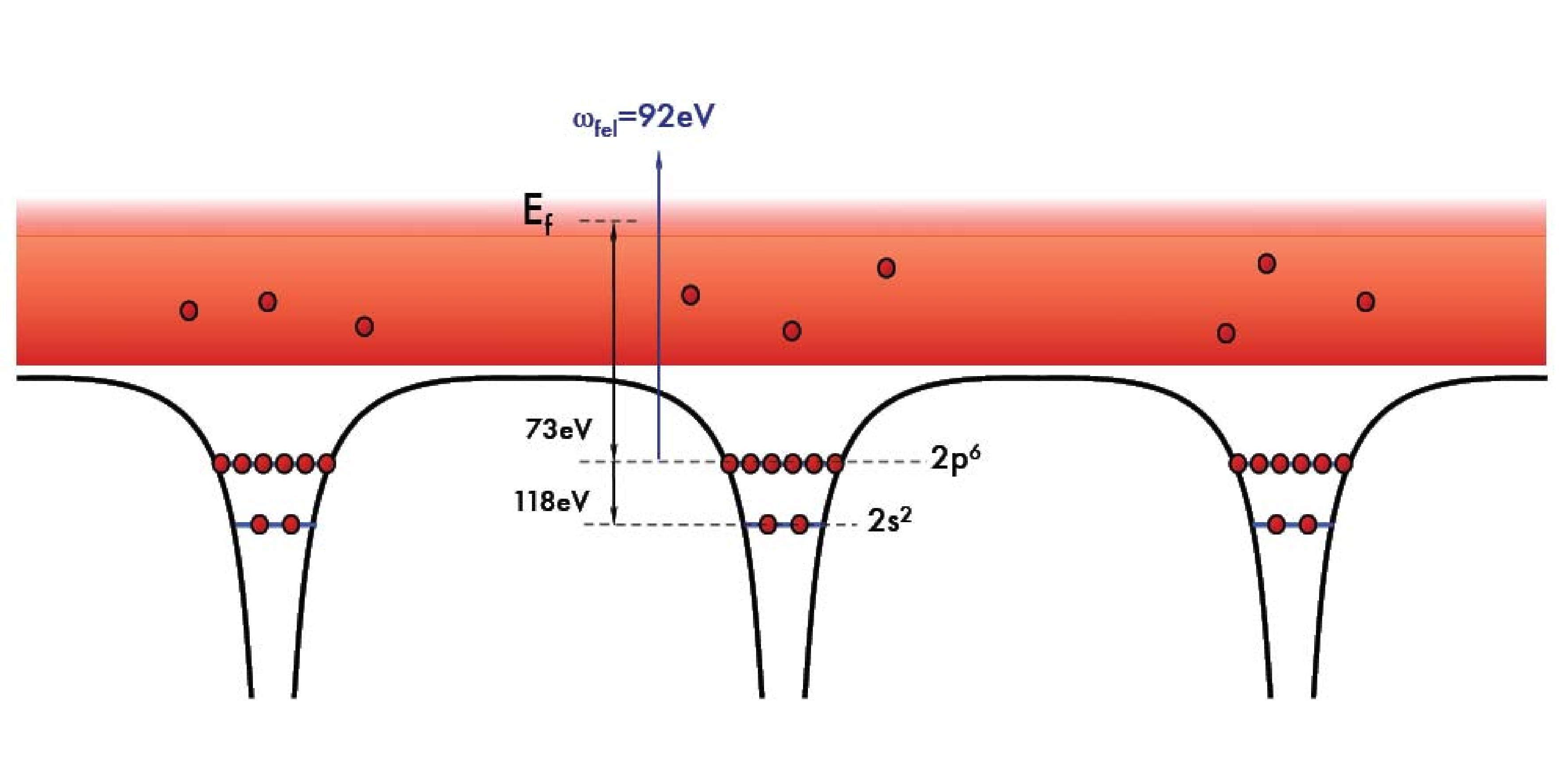

photo-ionizing one 2p electron from L shell

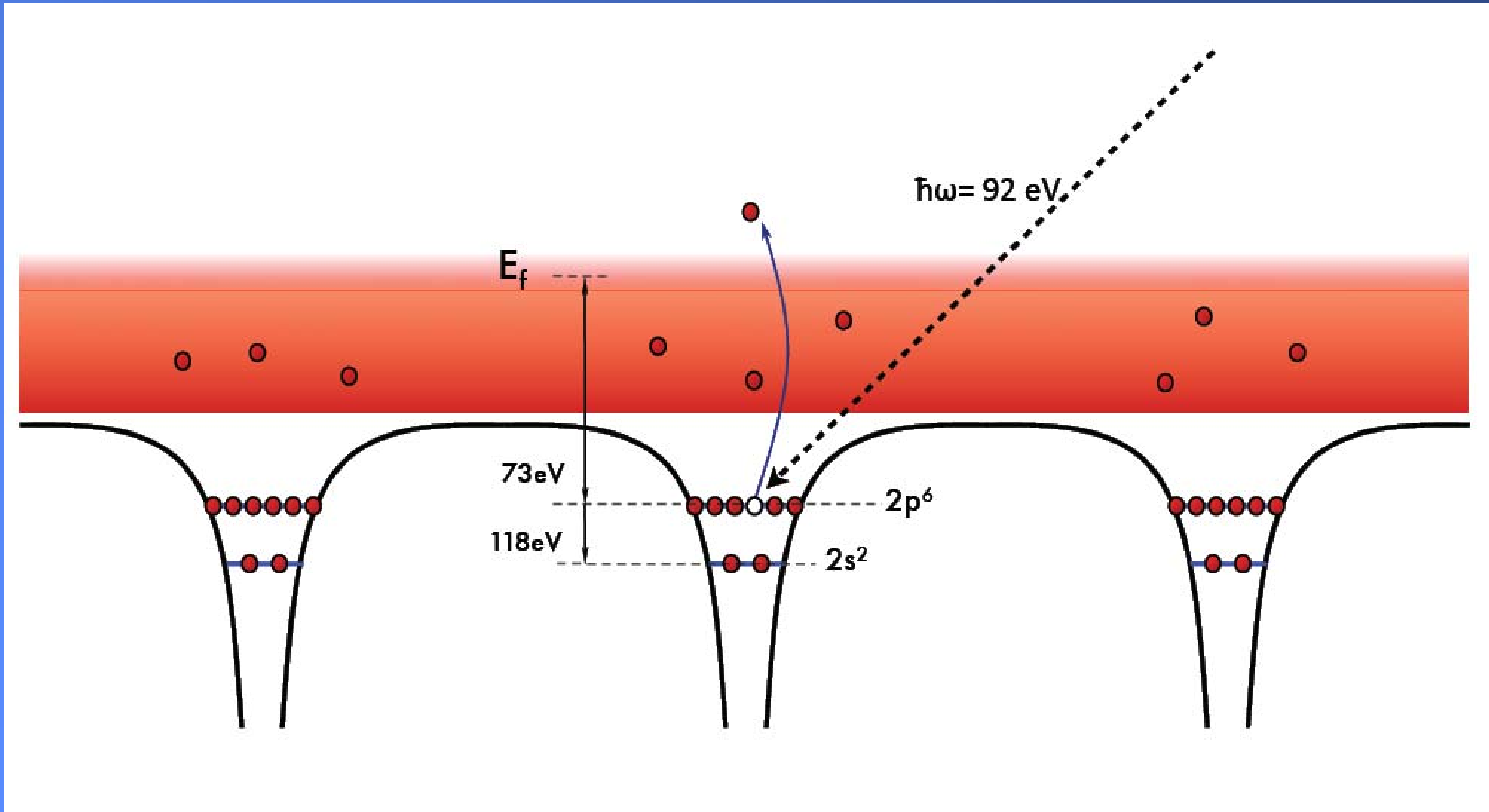

blue shift of the L edge; photo-ionization of more 2p electrons is not possible by 92-eV FEL photons

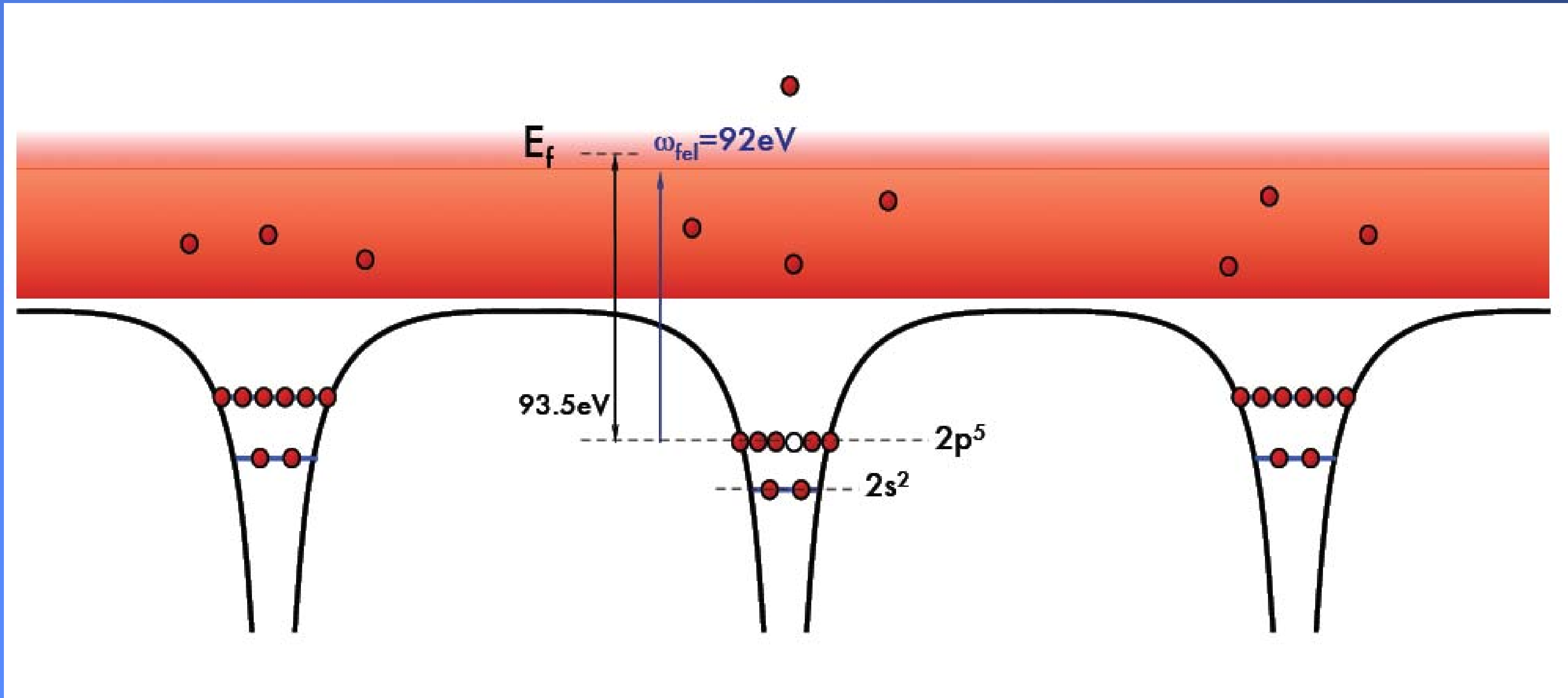

calculations: B. Nagler, S. Vinko et al.

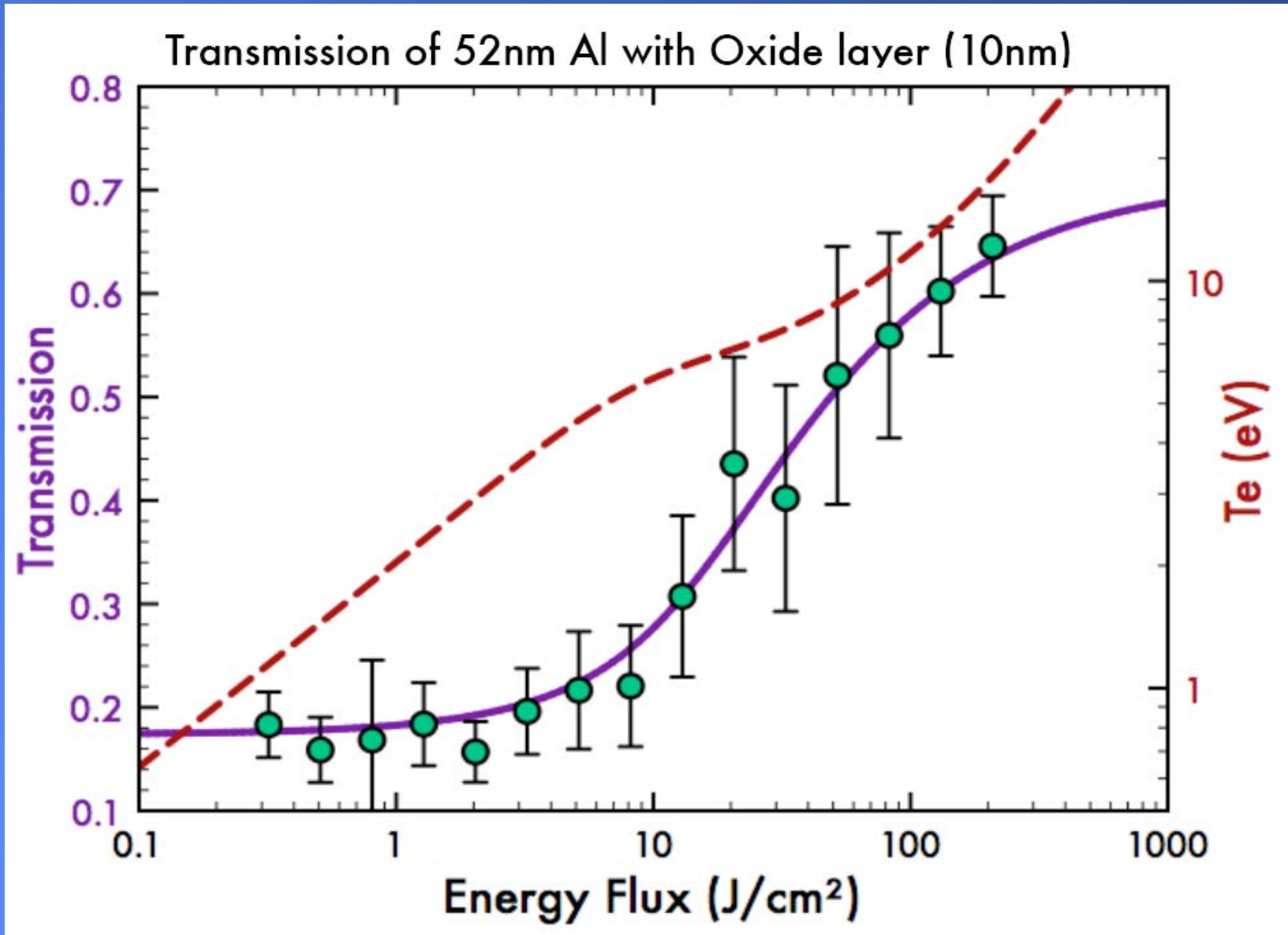

calculations: B. Nagler, S. Vinko et al.

NANOSCOPY LAB
IP-ASCR-Prague

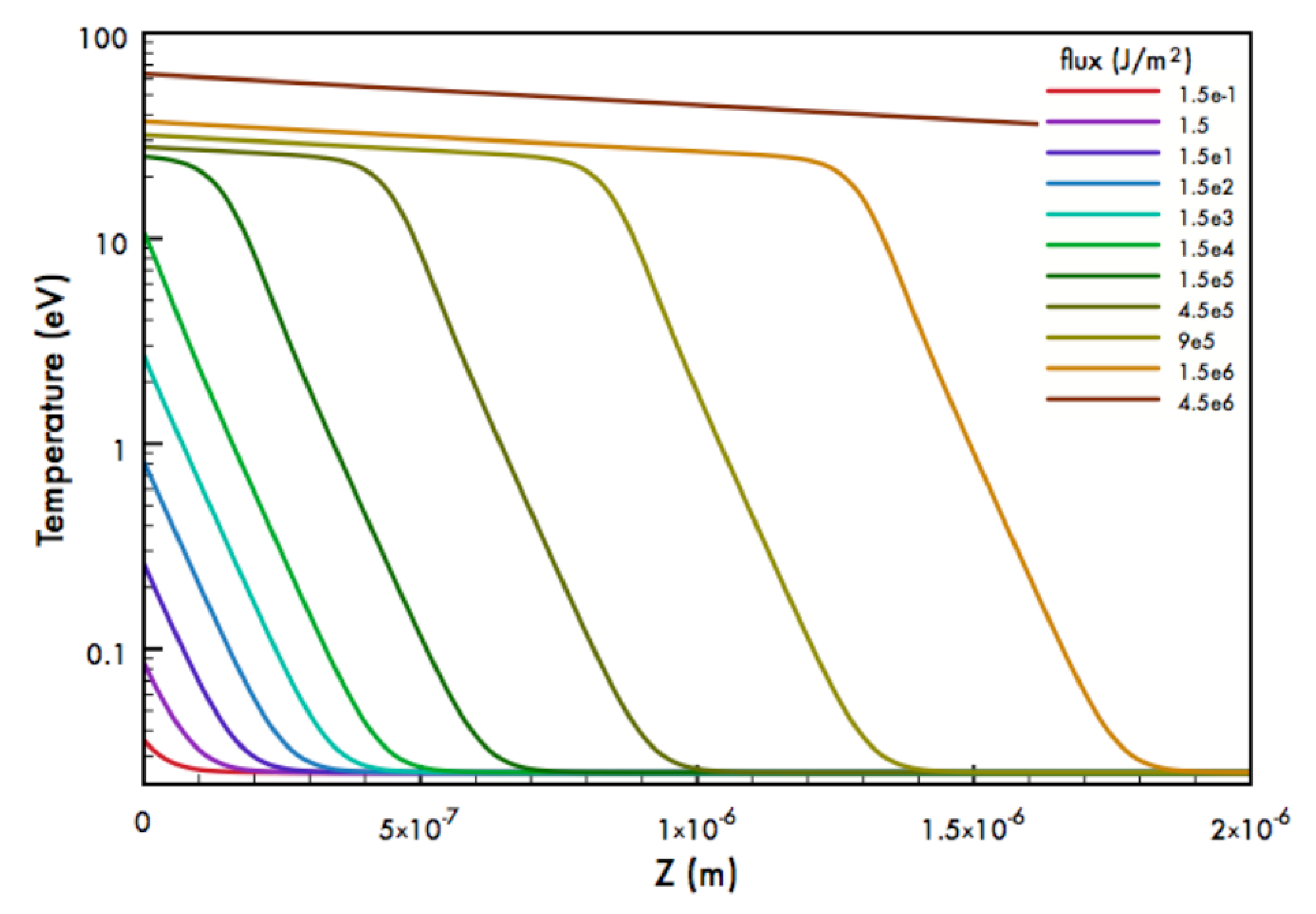

homogeneous heating is solving the problem of T_e and n_e gradients

PRL 104, 225001 (2010) PHYSICAL REVIEW LETTERS week ending 4 JUNE 2010

Electronic Structure of an XUV Photogenerated Solid-Density Aluminum Plasma

S. M. Vinko,[1,*] U. Zastrau,[2] S. Mazevet,[3] J. Andreasson,[4] S. Bajt,[5] T. Burian,[6] J. Chalupsky,[6] H. N. Chapman,[7,8] J. Cihelka,[6] D. Doria,[9] T. Döppner,[10] S. Düsterer,[5] T. Dzelzainis,[9] R. R. Fäustlin,[5] C. Fortmann,[10] E. Förster,[2] E. Galtier,[11] S. H. Glenzer,[10] S. Göde,[12] G. Gregori,[1] J. Hajdu,[4] V. Hajkova,[6] P. A. Heimann,[13] R. Irsig,[12] L. Juha,[6] M. Jurek,[14] J. Krzywinski,[15] T. Laarmann,[5] H. J. Lee,[15] R. W. Lee,[10] B. Li,[1] K.-H. Meiwes-Broer,[12] J. P. Mithen,[1] B. Nagler,[16] A. J. Nelson,[10] A. Przystawik,[12] R. Redmer,[12] D. Riley,[9] F. Rosmej,[11] R. Sobierajski,[17,14] F. Tavella,[5] R. Thiele,[12] J. Tiggesbäumker,[12] S. Toleikis,[5] T. Tschentscher,[18] L. Vysin,[6] T. J. Whitcher,[1] S. White,[9] and J. S. Wark[1]

NANOSCOPY LAB IP-ASCR-Prague

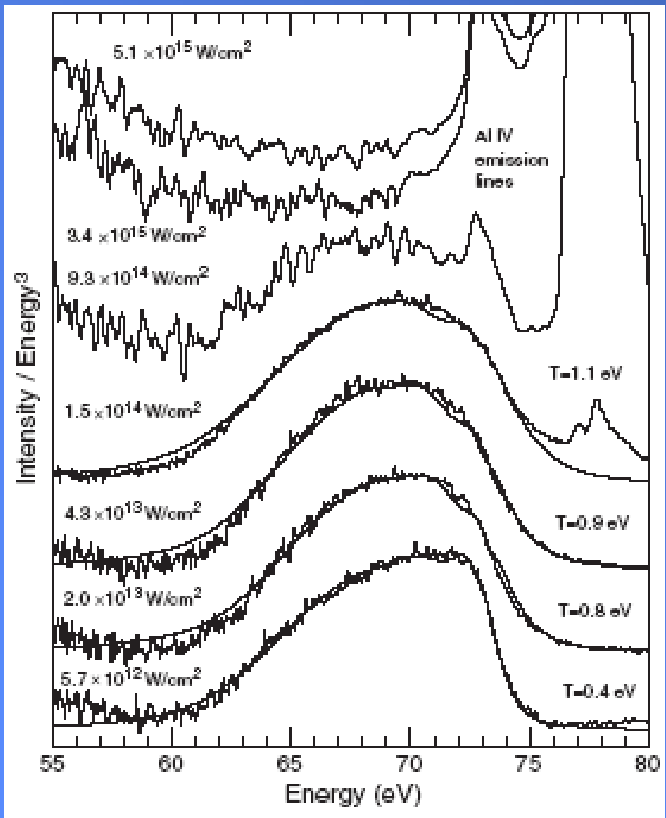

an example of „a dilute system“: low cross section and/or yield of the phenomenon investigated

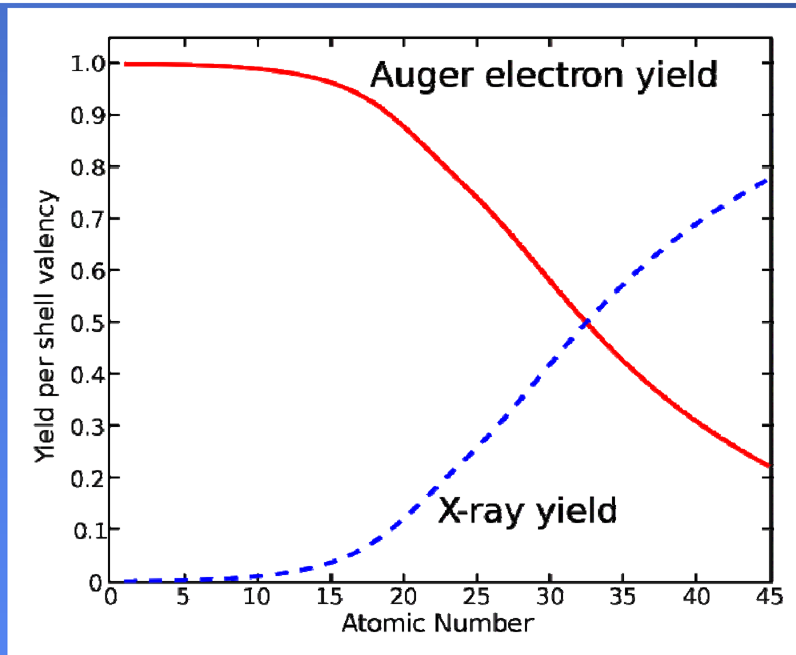

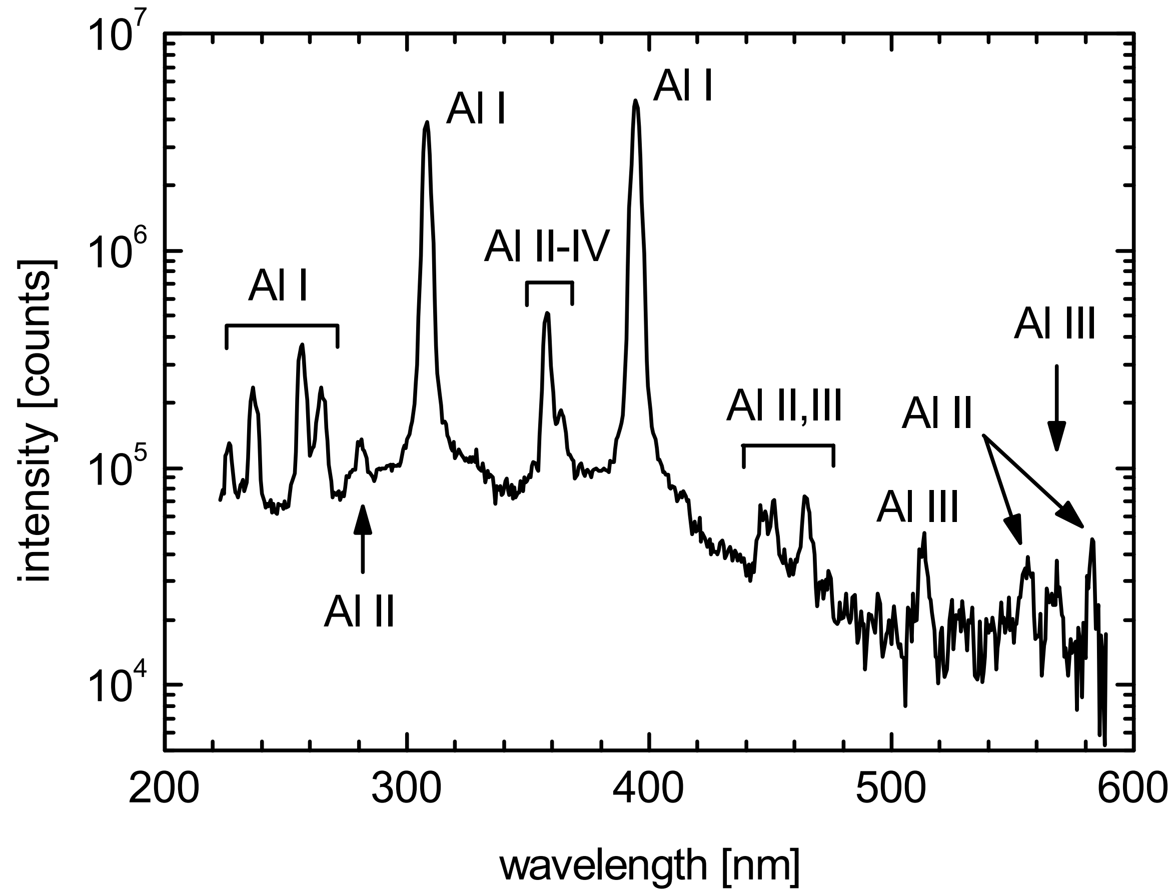

NANOSCOPY LAB IP-ASCR-Prague

OES of aluminium placed in the FLASH microfocus [10^{16} W/cm^2; J. Cihelka et al.: Optical emission spectroscopy of various materials irradiated by soft x-ray free-electron laser, *Proc. SPIE* 7361, 73610P (2009)]

Computer simulation of Al I emission using the code MARIA

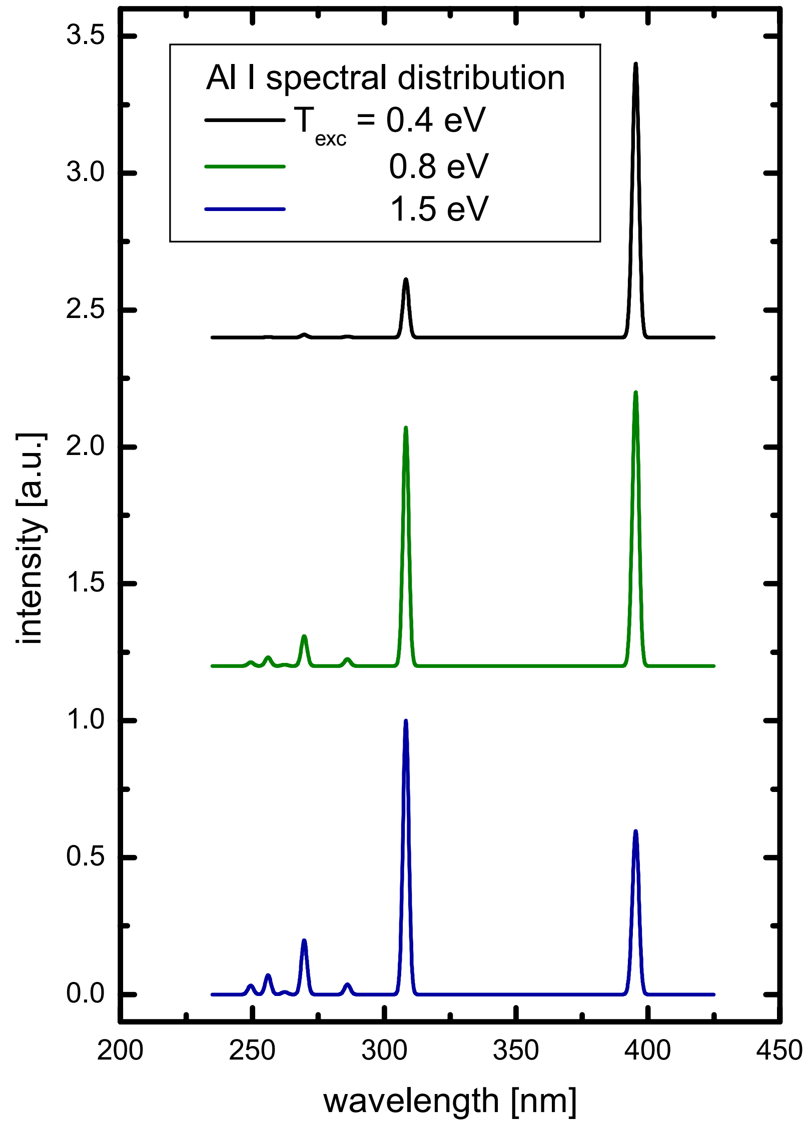

calculation: F. Rosmej, O. Renner

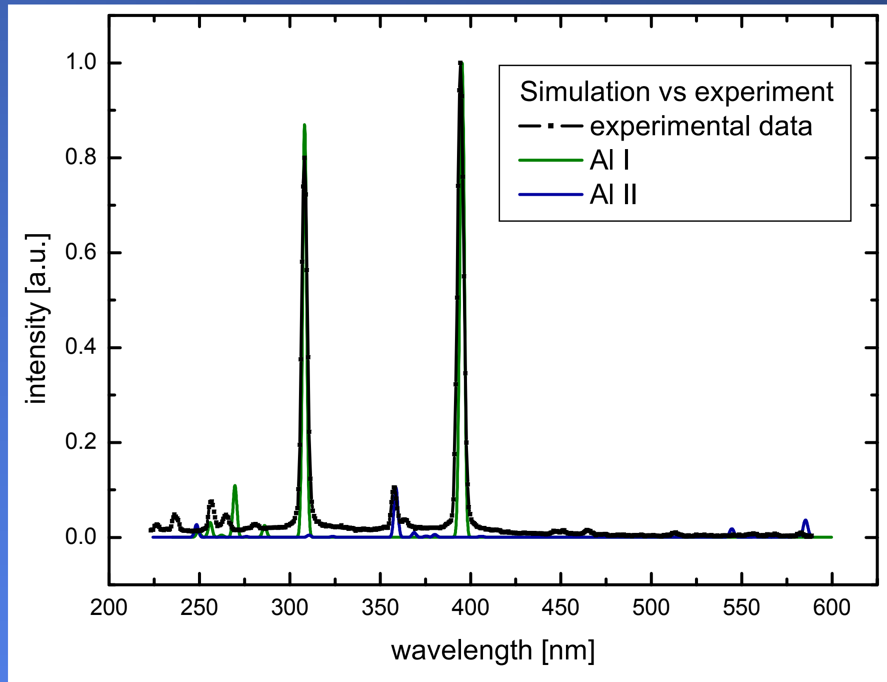

resulting excitation temperature is about 0.8 eV

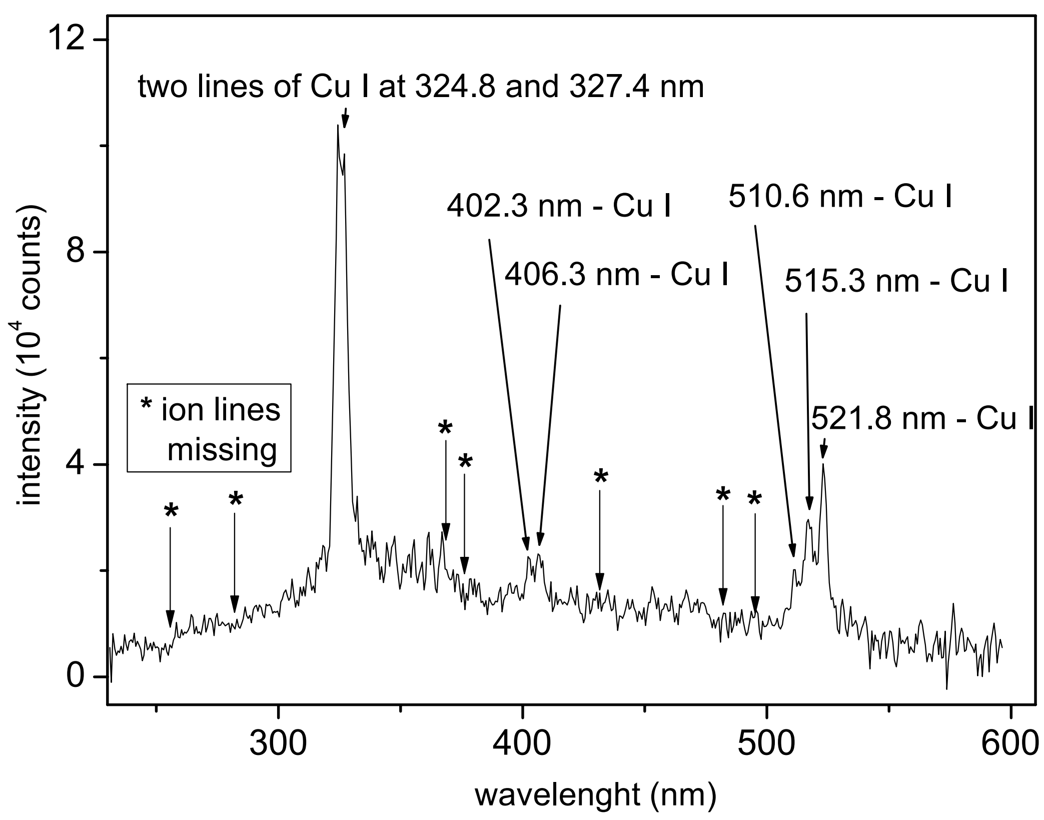

NANOSCOPY LAB
IP-ASCR-Prague

OES of copper massive target placed in the FLASH microfocus [10^{16} W/cm^2; J. Cihelka et al.: Optical emission spectroscopy of various materials irradiated by soft x-ray free-electron laser, *Proc. SPIE* 7361, 73610P (2009)]

Optical emission spectrum of Ce:YAG irradiated by 13.7-nm FLASH radiation focused at an irradiance of 10^{15} W/cm^2

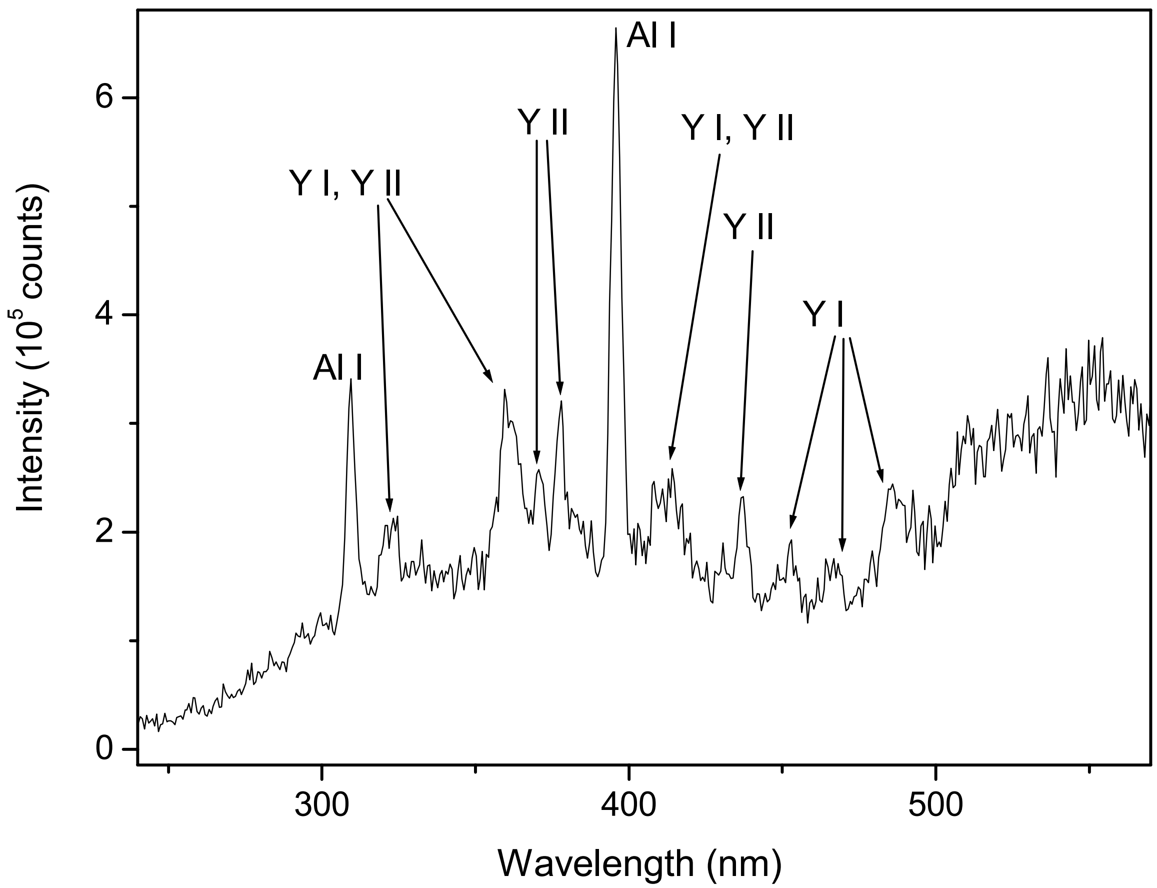

probing plasma by Thomson scattering

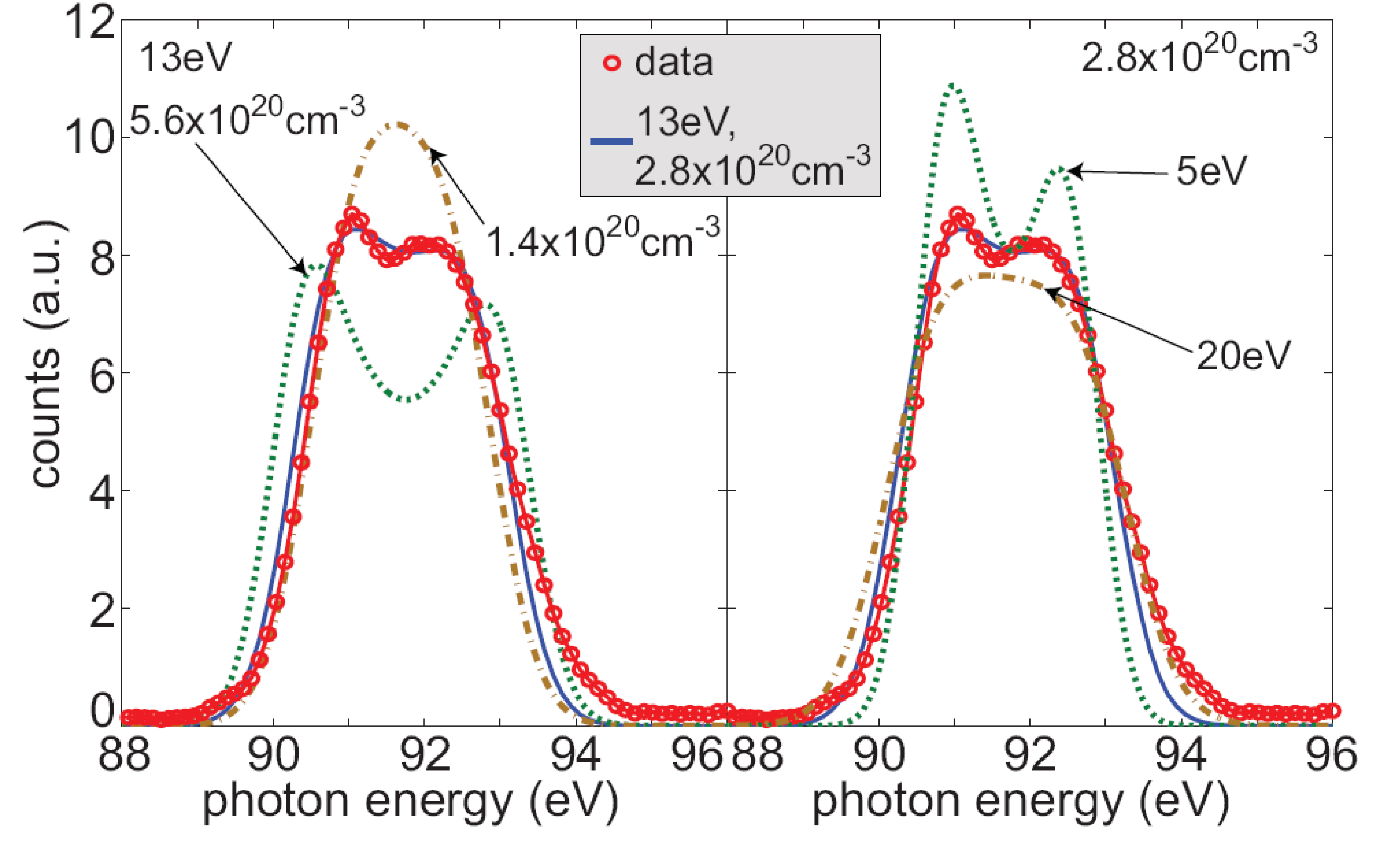

S. Toleikis et al.: one FALSH pulse heats and scatters (~8·10[13] W/cm²)

LCLS:SXR experimental setup

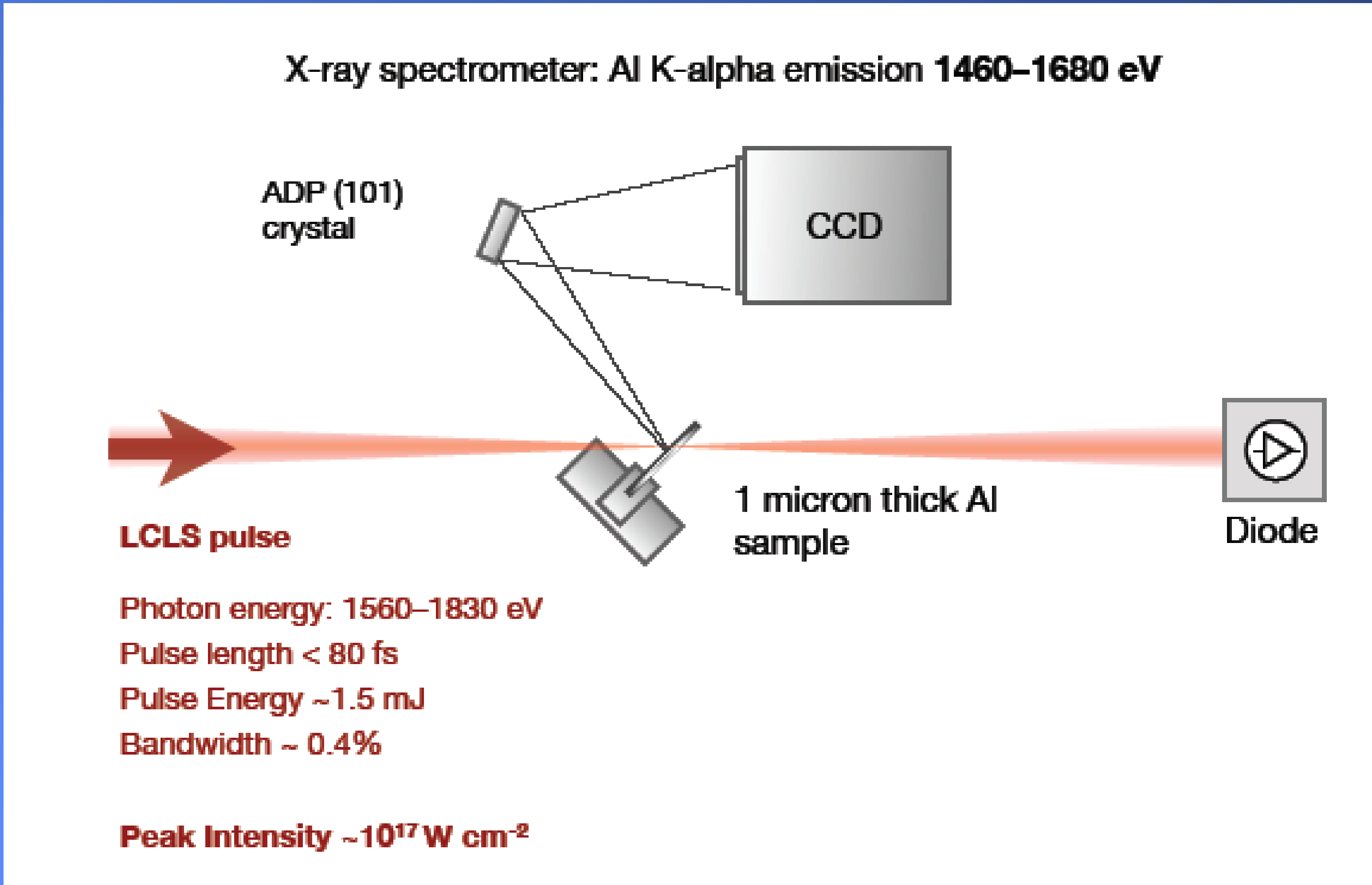

S. M. Vinko et al.: Creation and diagnosis of solid-density hot-dense matter with an X-ray free-electron laser, *Nature* 482, 59 (2012)

K-shell spectroscopy of Hot Dense Aluminium

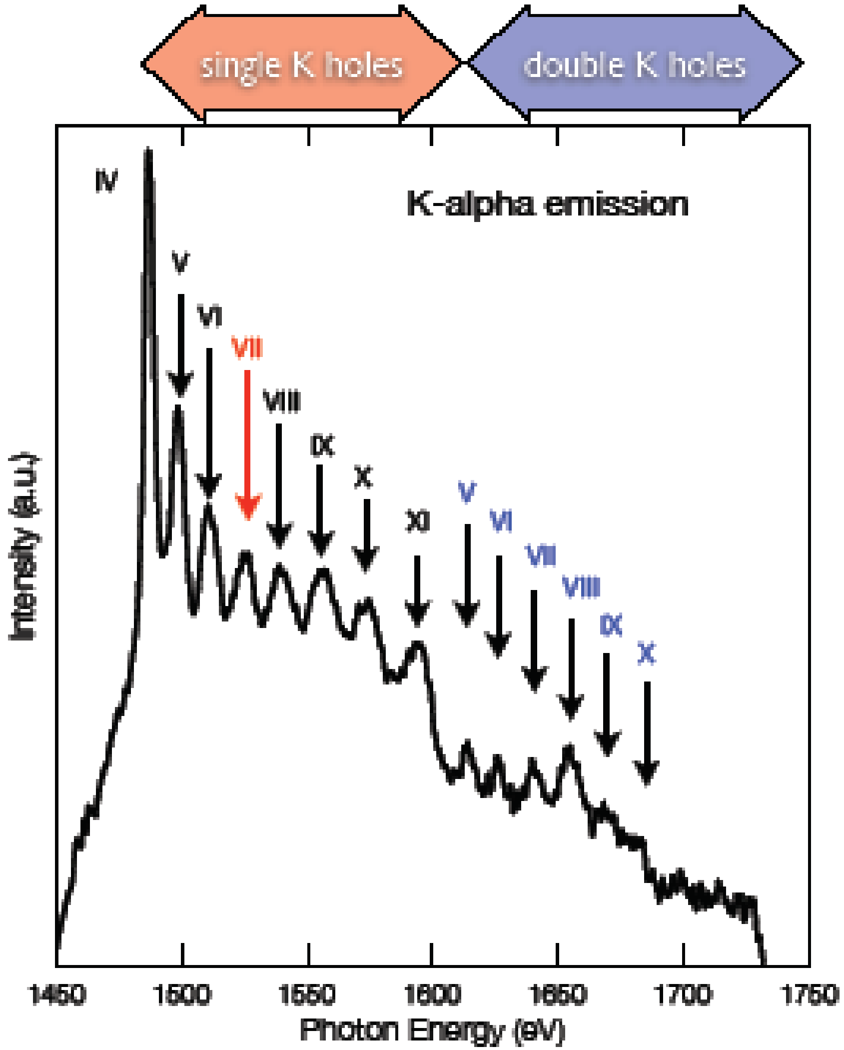

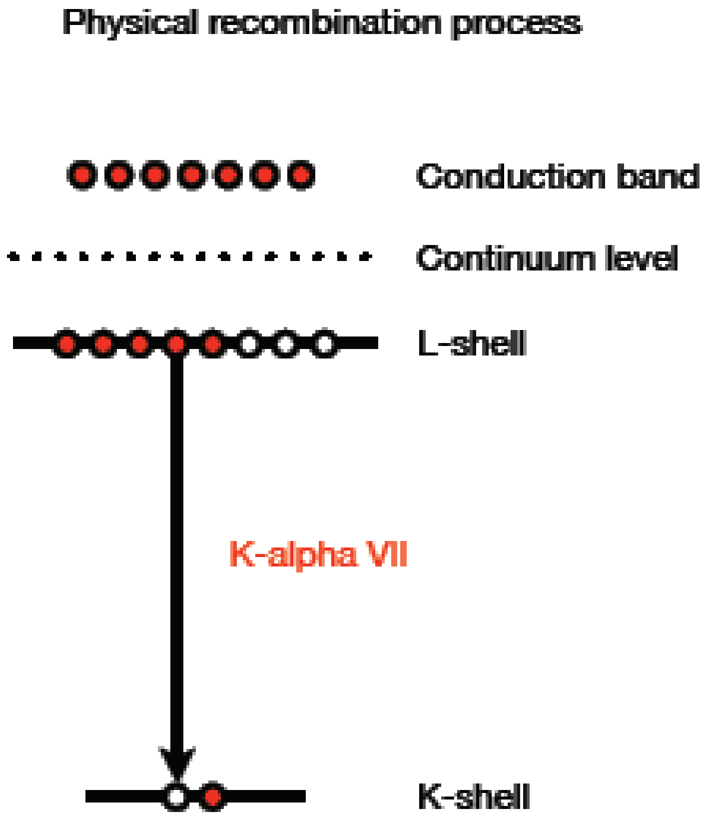

FEL photon energy: 1830 eV

Conclusions

- First experimental results looking at high-intensity X-ray FEL interaction with solid density Al samples: dynamics are very different to single-atom case;
- Electron collisional processes dominate the CSD, even in the presence of the intense X-ray pulse;
  - simulations indicate 'thermal' CSD within a fraction of the pulse
- Temperatures in excess of 150-200 eV achieved at solid densities;
- Absorption/heating determined by the ionized states, ground-state cross sections largely irrelevant!
- Emission spectrum generated by a quasi-monochromatic X-ray pulse is not necessarily representative of the CSD, but is sensitive to the K-edges of the excited system.

S. M. Vinko et al.: Creation and diagnosis of solid-density hot-dense matter with an X-ray free-electron laser, *Nature* **482**, 59 (2012)

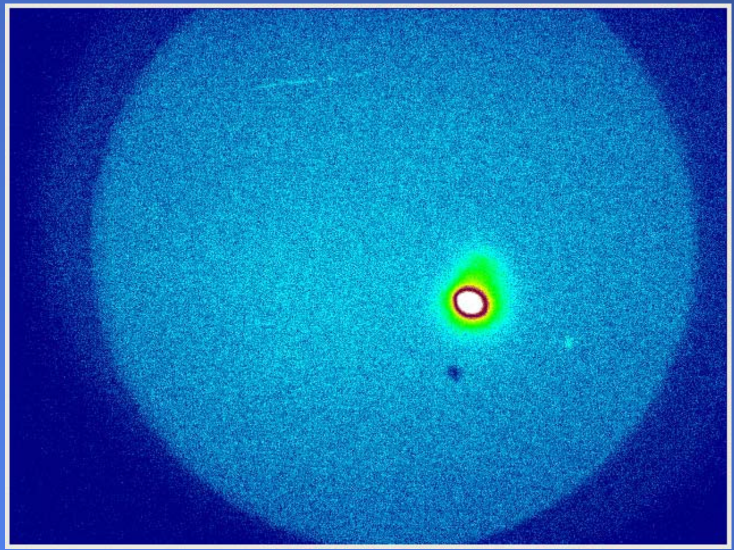

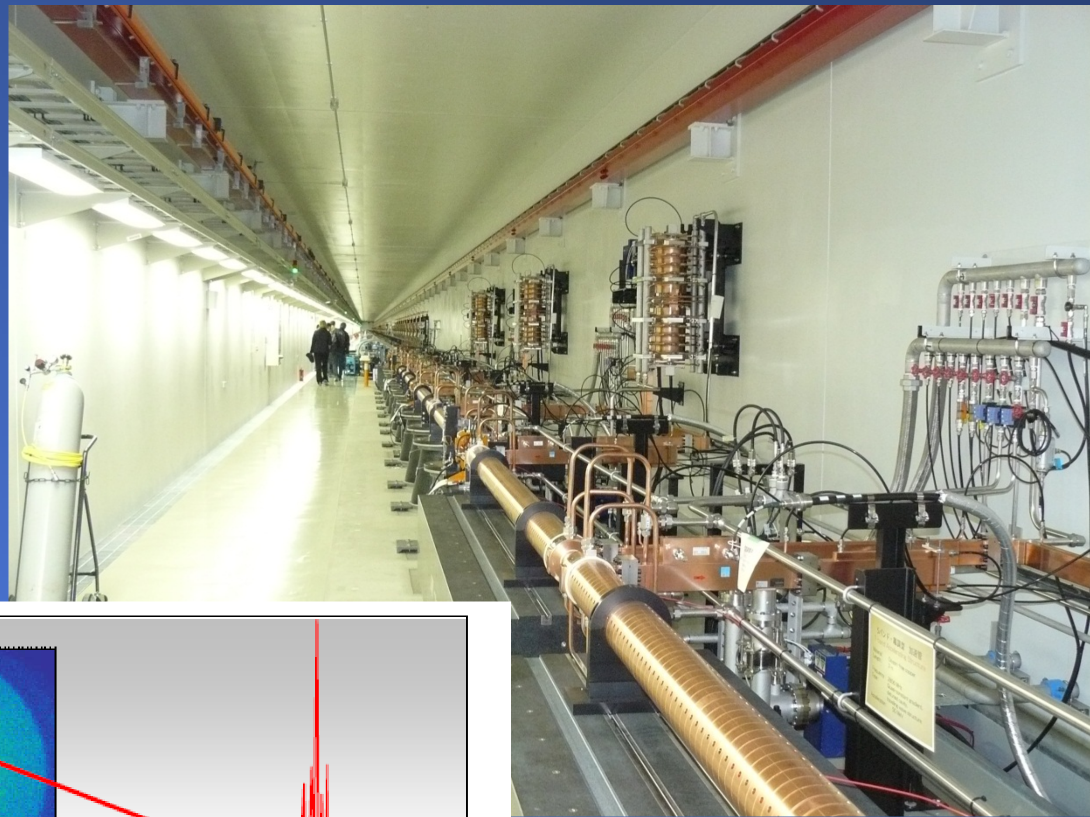

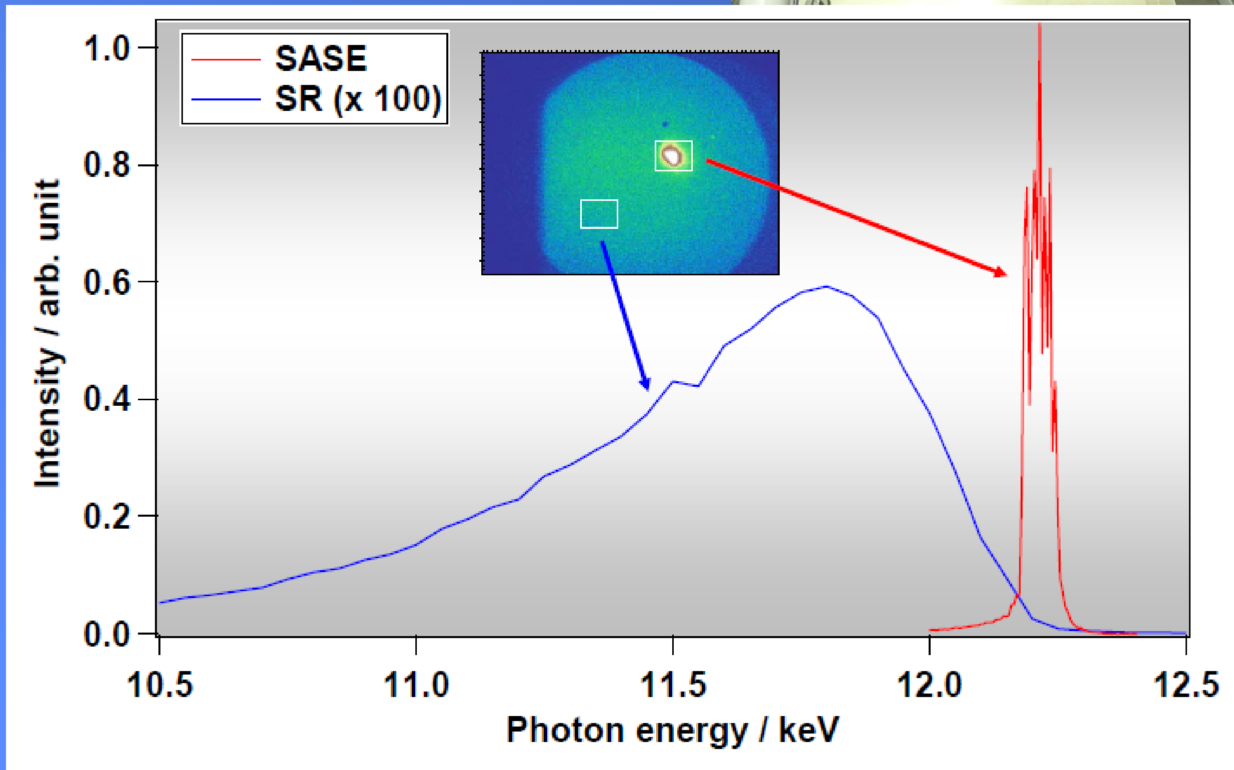

SACLA - SPring-8 Angstrom Compact free-electron LAser

Commissioned: June 2011

Currently lasing at 0.08 nm

ELI-Beamlines Facility near Prague

ELI Beamlines Facility laser

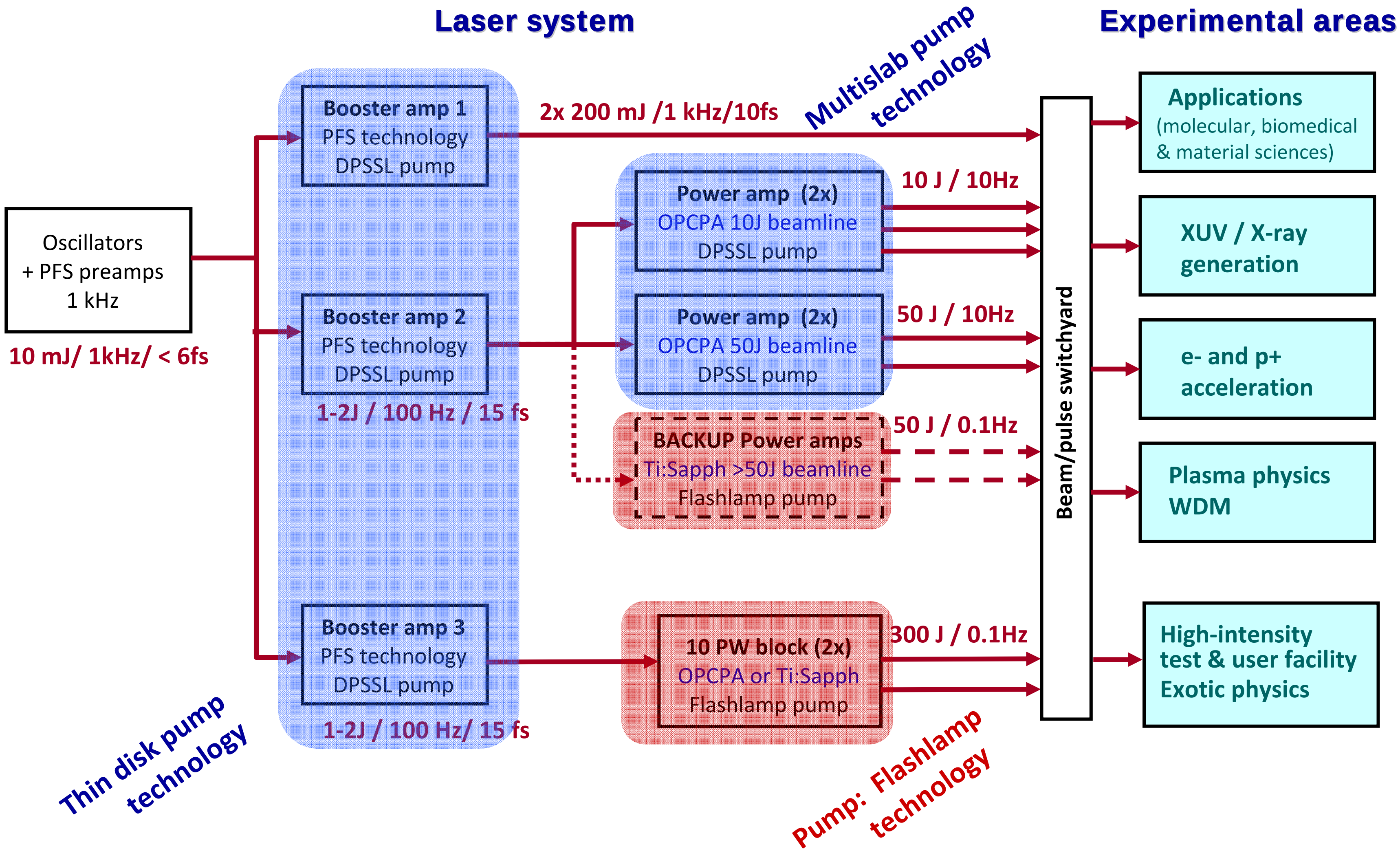

ELI-Beamlines mission

1. Generation of femtosecond secondary sources of radiation and particles
   - **XUV and X-ray sources (monochromatic and broadband)**
   - Accelerated electrons (2 GeV 10 Hz rep-rate, 100 GeV low rep-rate),
     protons (200-400 MeV 10 Hz rep-rate, >3 GeV low-rep-rate)
   - Gamma-ray sources (broadband)

2. Programmatic applications of the femtosecond secondary sources
   - Medical research including proton therapy
   - **Molecular, biomedical and material sciences**
   - **Physics of dense plasmas, WDM, laboratory astrophysics**

3. High-field physics experiments with focused intensities 10^{23}-10^{24} Wcm^{-2}
   - Exotic plasma physics (e.g. electron-positron pair plasma), non-linear QED

4. Participation in prototyping technologies for the high-intensity pillar

   Compression & coherent superposition of multi-10-PW ultrashort pulses

Summary

(1) Short-wavelength lasers interact with matter and plasmas in a different way than conventional, long-wavelength lasers.

(2) Unique states of matter (e.g., WDM) can be both created and probed by short-wavelength free-electron lasers.

(3) XUV/X-ray free-electron lasers produce from irradiated solids relatively unifom dense plasmas because of volumetric (caused by the short wavelength) and isochoric (resulting from delivering energy in ultra-short pulses) heating.

thank you for your attention